

UNIVERSIDADE ESTADUAL DE PONTA GROSSA  
SETOR DE CIÊNCIAS EXATAS E NATURAIS  
PROGRAMA DE PÓS-GRADUAÇÃO EM CIÊNCIAS

ELAHEH SAYARI

ANALYZING BURSTING SYNCHRONIZATION IN NEURAL NETWORK MODELS  
WITH EXTERNAL PULSED PERTURBATIONS  
ANÁLISE DA SINCRONIZAÇÃO DE RUPTURA EM MODELOS DE REDES NEURAIIS  
COM PERTURBAÇÕES PULSADAS EXTERNAS

PONTA GROSSA  
2024

ELAHEH SAYARI

ANALYZING BURSTING SYNCHRONIZATION IN NEURAL NETWORK MODELS  
WITH EXTERNAL PULSED PERTURBATIONS  
ANÁLISE DA SINCRONIZAÇÃO DE RUPTURA EM MODELOS DE REDES NEURAIS  
COM PERTURBAÇÕES PULSADAS EXTERNAS

Thesis presented to the Graduate Program in Sciences, concentration area Physics, of the Universidade Estadual de Ponta Grossa, in partial fulfillment of the requirements for the degree of Doctor in Science.

Advisor: Prof. Dr. Antonio Marcos Batista

PONTA GROSSA  
2024

S274 Sayari, Elaheh  
Analyzing bursting synchronization in neural network models wiht external pulsed perturbations / Elaheh Sayari. Ponta Grossa, 2024.  
58 f.

Tese (Doutorado em Ciências - Área de Concentração: Física), Universidade Estadual de Ponta Grossa.

Orientador: Prof. Dr. Antonio Marcos Batista.

1. Neural network. 2. Bursting synchronization. 3. Desynchronization. 4. External pulsed currents. 5. Plasticity. I. Batista, Antonio Marcos. II. Universidade Estadual de Ponta Grossa. Física. III.T.

CDD: 530

## TERMO DE APROVAÇÃO

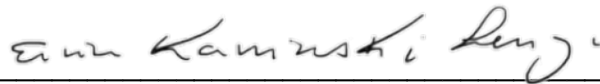
ELAHEH SAYARI

### ANALYSING BURSTING SYNCHRONIZATION IN NEURAL NETWORK MODELS WITH EXTERNAL PULSED PERTURBATIONS

Tese aprovada como requisito parcial para obtenção do grau de Doutor em Ciências, no Programa de Pós-Graduação em Ciências, Área de Concentração Física, da Universidade Estadual de Ponta Grossa, pela seguinte banca examinadora:

Orientador  \_\_\_\_\_

Dr. Antonio Marcos Batista – UEPG– Presidente



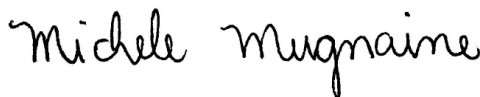
Dr. Ervin Kaminski Lenzi – UEPG - Titular



Dr. Eduardo Luis Brugnago – IFUSP – Titular



Dr. Silvio Luiz Thomaz de Souza – UFSJ – Titular



Dra. Michele Mugnaine – IFUSP – Titular

Ponta Grossa, 18 de janeiro de 2024.

## **ACKNOWLEDGEMENTS**

I am deeply thankful to my family, especially my husband, Mehdi, my mother, Azra, and my son, Elyas, for their love and support during this study. Without their encouragement and motivation, I would not have been able to complete this journey.

I am deeply grateful to my advisor, Prof. Dr. Antonio Marcos Batista, for his unwavering support and guidance throughout my PhD program. His expertise and patience have been invaluable to me and have played a crucial role in the success of this thesis.

I would like to thank my professors and colleagues at 105 Group Science for their support and collaboration during my research.

I also thank Coordination for the Improvement of Higher Education Personnel (CAPES) for supporting me financially to be able to study and live in Ponta Grossa.

*This thesis work is dedicated to my husband, Mehdi, who has been a constant source of support and encouragement during the challenges of study and life. I am truly thankful for having you in my life. Also, this work is dedicated to my son, Elyas. You have made me stronger, better and more fulfilled than I could have ever imagined. I love you to the moon and back. Furthermore, this work is dedicated to my parents and sister, Elham, who have always loved me unconditionally and whose good examples have taught me to work hard for the things that I aspire to achieve.*

## ABSTRACT

The brain has a complex structure and is located at the center of the nervous system. At the cellular level, the nervous system has neurons that send signals rapidly and precisely to other cells. Dynamical features of neurons, bursting synchronization and desynchronization, in a neural network can not only be associated with memory and consciousness, but also be related to unhealthy neural behaviors. To regulate abnormal neural activities, for instance, in patients with neurological disorders, such as epilepsy, Alzheimer's, and Parkinson's diseases, external pulsed currents, such as deep brain stimulation, can influence the bursting synchronous behavior in a neural network and cause alterations in neural spiking activities. Throughout this thesis, the main goals are to demonstrate the emergence of bursting synchronization and desynchronization in two different neural networks, and also to show the effect of external periodic and random pulsed currents on neural activities related to pathological synchronous behavior in these neural networks. Firstly, a neural network model containing Rulkov's neurons connected by means of a random structure, Erdős-Rényi model, is built. The formation and destruction of bursting synchronization in a random neural network model with burst-timing-dependent plasticity are investigated. We study the effect of two external pulsed currents, periodic and random pulses, on bursting synchronization in a plastic neural network. Secondly, a neural network composed of coupled subnetworks with small-world properties according to one human cerebral cortex, limbic system, and brain stem is considered. The burst synchronization and desynchronization in the network under external periodic and random pulsed perturbations are studied. Overall, the results of this thesis show that the burst-timing-dependent plasticity and the synaptic interaction between presynaptic and postsynaptic neurons can exhibit the formation and destruction of bursting neural synchronization in network models. The external pulsed currents can be an effective method to suppress bursting neural synchronization in neural networks.

**Keywords:** Neural Network, Bursting Synchronization, Desynchronization, External Pulsed Currents, Plasticity.

## RESUMO

O cérebro é uma estrutura complexa que está localizado no centro do sistema nervoso. No nível celular, o sistema nervoso possui neurônios que enviam sinais de forma rápida e precisa para outras células. As características dinâmicas dos neurônios, sincronização e dessincronização intermitentes, em uma rede neural, podem não apenas estar associadas à memória e à consciência, mas também estar relacionadas a comportamentos neurais prejudiciais. Para regular atividades neurais anormais, por exemplo, em pacientes com distúrbios neurológicos, como epilepsia, Alzheimer e Parkinson, correntes pulsadas externas, como estimulação cerebral profunda, podem influenciar o comportamento síncrono de disparos em uma rede neural. Ao longo desta tese, os principais objetivos são demonstrar o surgimento de sincronização e dessincronização dos disparos em duas redes neurais diferentes. Também mostrar o efeito de correntes externas periódicas e pulsadas aleatórias em atividades neurais relacionadas ao comportamento síncrono patológico nessas redes neurais. Primeiramente, um modelo de rede neural contendo os neurônios de Rulkov conectados por meio de uma estrutura aleatória, modelo Erdős-Rényi, é construído. Nesta rede estudamos a influência da plasticidade dependente do tempo nos disparos neuronais, bem como os efeitos de correntes pulsadas externas, pulsos periódicos e aleatórios na sincronização. Na sequência, analisamos uma rede neural composta de sub-redes acopladas com propriedades de mundo pequeno de acordo com o córtex cerebral humano, sistema límbico e tronco cerebral. Em geral, os resultados desta tese mostram que a plasticidade dependente do tempo e a interação sináptica entre neurônios pré-sinápticos e pós-sinápticos contribuem para a formação e destruição de sincronização neural, bem como que as correntes pulsadas externas podem ser eficazes para suprimir a sincronização em redes neurais.

**Palavras-chave:** Rede Neural, Sincronização, Dessincronização, Correntes Pulsadas Externas, Plasticidade.



## LIST OF FIGURES

Figure 2.1 – Basic anatomy of a neuron. A typical neuron can be separated into three basic regions: the soma including nucleus, dendrites and axon including axon terminals (16). . . . .	16
Figure 2.2 – Cell membrane representation. The cell membrane contains proteins functioning as channels that allow the ions to move through it. The ion flux changes the concentration of the intracellular and extracellular sides, inducing variations in the membrane potential. . . . .	16
Figure 2.3 – Typical action potential of the neuron, identifying the resting state, depolarization, repolarization, and hyperpolarization. The threshold potential is indicated by the dashed line. . . . .	17
Figure 2.4 – Schematic representation of the (a) chemical and (b) electrical synapses. . . . .	18
Figure 2.5 – Time evolution of (a) the fast variable ( $x_t$ ) and (b) the slow variable ( $y_t$ ), where the red circles correspond to the bursting beginning. $x_0$ and $y_0$ are randomly selected from the interval $[-2, 2]$ and $[-4, 0]$ , respectively, $\alpha = 4.1$ , $\delta = 0.001$ , and $\beta = 0.001$ . . . . .	20
Figure 2.6 – Time evolution of the fast variable $x_k$ for (a) $\alpha = 2.3$ , (b) $\alpha = 3.0$ , (c) $\alpha = 4.1$ , and (d) $\alpha = 4.5$ . The red circles show the maximum value of the slow variable $y_k$ . $x_0$ and $y_0$ are randomly selected from the interval $[-2, 2]$ and $[-4, 0]$ , respectively, $\delta = 0.001$ and $\beta = 0.001$ . . . . .	21
Figure 2.7 – Illustration of the Königsberg bridges. The Pregel River ramifications form two islands $A$ and $D$ , which are connected to the city by the 7 bridges $a$ , $b$ , $c$ , $d$ , $e$ , $f$ , and $g$ . . . . .	21
Figure 2.8 – Examples of regular graphs for 10 nodes linked to their (a) 2 nearest neighbors, (b) 4 nearest neighbors and (c) all the possible neighbors to form a global network (complete network). . . . .	23
Figure 2.9 – Examples of random graphs for 10 nodes with (a) $p_r = 0.05$ , (b) $p_r = 0.5$ and (c) $p_r = 1$ . . . . .	23
Figure 2.10 – Examples of Watts-Strogatz graphs for 10 nodes linked to their 4 nearest neighbors with (a) $p_{ws} = 0$ as a regular network, (b) $p_{ws} = 0.5$ as a small-world network and (c) $p_{ws} = 1$ as a random network. The small-world regime is achieved between the extremes of order and randomness. . . . .	24
Figure 2.11 – Examples of Newman-Watts graphs for 10 nodes connected to their 4 nearest neighbors with (a) $p_{ws} = 0$ as a regular network, (b) $p_{ws} = 0.5$ as a small-world network and (c) $p_{ws} = 1$ as a network that is no longer in the small-world regime. . . . .	25

Figure 2.12 – (a) Periodic pulsed current for $I_0 = 10 \mu\text{A}/\text{cm}^2$ , $\tau = 1.5 \mu\text{A}/\text{cm}^2$ , $\Delta t_{p_1} = 2$ ms, and $\Delta t_{p_2} = 2$ ms, and (b) random pulsed perturbation for $I_0 = 10 \mu\text{A}/\text{cm}^2$ , $\tau = 1.5 \mu\text{A}/\text{cm}^2$ , and $\Delta t_r$ randomly distributed in the interval $[0, 20]$ ms. . . . .	29
Figure 2.13 – The Deep Brain Stimulation system consists of three components: the lead, the extension wire, and the neurostimulator. . . . .	29
Figure 3.1 – Change on synaptic weight as a function of the time latency between the burst-start events of two connected neurons. Bursts starting close together cause synapse potentiation, while large burst latency causes depression. . .	33
Figure 3.2 – Time evolution of the mean synaptic weight (red line) and order parameter (black line) for (a) $W_0 = 0$ and (b) $W_0 = 0.1$ . It is observed that the potentiation begins before occurring bursting synchronization. . . . .	34
Figure 3.3 – Mean synaptic weight as a function of the initial synaptic weight. The curve is separated into three parts: $W_0 \leq 0.045$ , $0.045 < W_0 < 0.055$ , and $W_0 \geq 0.055$ . The potentiation is preferred more than depression. . . . .	34
Figure 3.4 – Time-averaged Kuramoto order parameter as a function of the initial synaptic weight value for before (initial state in black line) and after (final state in red line) applying the BTDP rule. . . . .	35
Figure 3.5 – $\Delta t_{p_2} \times \Delta t_{p_1}$ for (a) $\tau = 0.3 \mu\text{A}/\text{cm}^2$ and (b) $\tau = 0.5 \mu\text{A}/\text{cm}^2$ with $I_0 = 8 \mu\text{A}/\text{cm}^2$ to represent $\bar{R}$ in color scale for the plastic network under a periodic external current. Depending on the time duration, synchronous behavior can be suppressed in the random network. . . . .	37
Figure 3.6 – Mean order parameter (color scale) in the parameter space $\tau \times I_0$ of coupled neurons under a random pulsed perturbation with $\Delta t_r$ randomly distributed in the interval $[0, 20]$ ms. It is not observed a significant alteration in the synchronization by varying $I_0$ . . . . .	37
Figure 4.1 – Illustration of cerebral cortex located at the cortical regions, limbic system located at the non-cortical regions, and brain stem in the brain. . . . .	39
Figure 4.2 – Connectome in the direction of the cuts: $y$ (coronal), $x$ (sagittal), and $z$ (axial), respectively, for a healthy subject. The color bar indicates the amount of weights described as the number of fibers. Only 15% of the connections are considered, due to the fact that the graphs are very dense. $L$ and $R$ indicate the left and right hemispheres, respectively. $P$ and $A$ depict the posterior and anterior of the brain, respectively. . . . .	39
Figure 4.3 – Structural connection matrix related to the 83 areas in the brain of a healthy human. The areas start from 1 to 41 for the right hemisphere, from 42 to 82 for the left hemisphere, and with the number 83 for the brainstem. . . . .	40

Figure 4.4 – Time-averaged order parameter (color bar) as a function of $c$ (chemical synapses) in the interval $[0, 0.05]$ and $e$ (electrical synapses) in the range $[0, 0.1]$ of the human’s brain areas during $10^6$ iterations. . . . .	42
Figure 4.5 – Averaged order parameter of the human’s brain network under a periodic pulse with $I_0 = 8 \mu\text{A}/\text{cm}^2$ and $\tau = 0.1 \mu\text{A}/\text{cm}^2$ in the parameter space $\Delta t_{p_2} \times \Delta t_{p_1}$ varying in the interval $[1, 100]$ ms for the synchronized point $e = 0.1$ and $c = 0.05$ . . . . .	43
Figure 4.6 – Time-averaged order parameter of the whole brain network grouped into regions from (a) 1 to 34, (b) 35 to 41, (c) 42 to 75, and (d) 76 to 82. A periodic pulsed current with $I_0 = 8 \mu\text{A}/\text{cm}^2$ and $\tau = 0.1 \mu\text{A}/\text{cm}^2$ in the parameter space $\Delta t_{p_2} \times \Delta t_{p_1}$ varying in the interval $[1, 100]$ ms for $e = 0.1$ and $c = 0.05$ , which indicates the bursting synchronization, is considered. .	44
Figure 4.7 – Time-averaged order parameter of the region 83 by considering a periodic pulsed perturbation with $I_0 = 8 \mu\text{A}/\text{cm}^2$ , and $\tau = 0.1 \mu\text{A}/\text{cm}^2$ in the parameter space $\Delta t_{p_2} \times \Delta t_{p_1}$ varying in the interval $[1, 100]$ ms for $e = 0.1$ and $c = 0.05$ indicating the burst synchronous behavior. . . . .	44
Figure 4.8 – Averaged order parameter of the whole brain network under a random pulsed current as a function of $\tau$ and $\Delta t_r$ changing in the interval $[0, 4] \mu\text{A}/\text{cm}^2$ and $[20, 100]$ ms, respectively, for $I_0 = 8 \mu\text{A}/\text{cm}^2$ , $e = 0.1$ , and $c = 0.05$ . . . .	45
Figure 4.9 – Time-averaged order parameter of the four cortical regions of the brain network from (a) 1 to 34, (b) 35 to 41, (c) 42 to 75, and (d) 76 to 82, by considering a random pulsed perturbation with $\tau$ and $\Delta t_r$ in the interval $[0, 4] \mu\text{A}/\text{cm}^2$ and $[20, 100]$ ms, respectively, for $I_0 = 8 \mu\text{A}/\text{cm}^2$ , $e = 0.1$ , and $c = 0.05$ . . . . .	45
Figure 4.10 – Time-averaged order parameter of the region 83 of the brain network under a random pulsed current for $\tau$ and $\Delta t_r$ selected from the interval $[0, 4] \mu\text{A}/\text{cm}^2$ and $[20, 100]$ ms, respectively. It is considered $I_0 = 8 \mu\text{A}/\text{cm}^2$ , $e = 0.1$ , and $c = 0.05$ . . . . .	46

## CONTENTS

<b>1 INTRODUCTION</b> . . . . .	<b>11</b>
<b>2 BASIC CONCEPTS</b> . . . . .	<b>15</b>
2.1 NEURON, ACTION POTENTIAL AND SYNAPSES . . . . .	15
2.2 NURON MODEL . . . . .	19
2.3 GRAPH THEORY AND COMPLEX NETWORKS . . . . .	20
2.4 PHASE SYNCHRONIZATION . . . . .	24
2.5 EXTERNAL PULSED PERTURBATIONS . . . . .	28
<b>3 RESEARCH AREA 1</b> . . . . .	<b>31</b>
3.1 RANDOM NETWORK OF RULKOV'S NEURONS . . . . .	31
3.2 RESULTS . . . . .	32
3.2.1 Bursting Synchronization Induced by Burst-Timing-Dependent Plasticity (BTDP) . . . . .	32
3.2.2 Effects of External Pulsed Perturbations in Bursting Synchronous Behavior . . . . .	36
<b>4 RESEARCH AREA 2</b> . . . . .	<b>38</b>
4.1 NETWORK OF SMALL-WORLD NETWORKS MODEL . . . . .	38
4.2 RESULTS . . . . .	41
4.2.1 Burst Synchronization without Pulses . . . . .	41
4.2.2 Applying External Pulsed Perturbations in Bursting Synchronization . . . . .	42
<b>5 FINAL REMARKS</b> . . . . .	<b>47</b>
<b>REFERENCES</b> . . . . .	<b>49</b>

## 1 INTRODUCTION

Synchronization is a phenomenon that occurs in many systems in the nature (1). In the 17th century, this phenomenon was recognized by Christiaan Huygens when two weakly coupled pendulum clocks synchronized in-phase (2). After that, this phenomenon was reported in a wide range of biological systems (3–5), in the rhythmic flashing of fireflies (6), in the crickets which synchronize their chirps by responding to the preceding chirp of their neighbors (7), and also in the action potentials of the nervous system (8,9). In the context of neuroscience, synchronization plays a key role for temporal coordination of neural activity in neural networks (8). Also, various researches have reported the importance of synchronization for performing cognitive functions (10, 11), such as memory (8), conscious perception (12, 13), and motor coordination (14), as well as in processing and binding information in the mammalian brain (15). However, abnormal levels of synchronization have been associated with unhealthy neural behaviors (16). A high degree of synchronization is observed in epileptic seizures (17), where seizure episodes are generated by an increase in the synchronization of some groups of neurons, and in Parkinson's disease, where there is an excessive synchronization in basal ganglia (18, 19). Reduced levels of synchronization among cortical areas can be found in brain disorders such as autism (20) and Alzheimer's disease (21). Due to this fact, there is a great interest in understanding the factors that may contribute to the emergence of synchronization and desynchronization in neural networks.

The brain is one of the most important organs in the body that is located at the centre of the nervous system (22). The nervous system is responsible for receiving stimuli from sensory receptors and sends them to the brain and spinal cord, as well as to conduct impulses back to other parts of the body (23). At the cellular level, the nervous system has approximately 100 billion neurons. The neurons are connected to each other by axons to form a neural network and send signals rapidly and precisely to other cells (24). The signals are sent in the form of electrochemical impulses through different mechanisms by means of synapses (25). The synapses within the brain can be divided into two general classes: electrical synapses and chemical synapses. The chemical synapses can be excitatory or inhibitory. Smith and Perede (26) demonstrated that chemical synaptic activity modulates nearby electrical synapses. They provided evidence that chemical transmission interacts with electrical synapses to regulate the conductance. Kopell and Ermentrout (27) reported that chemical and electrical synapses perform complementary roles in the synchronous behavior of neural networks.

Each node in a neural network can be described by a map-based model like the Rulkov model, which is a two-dimensional iterated map proposed by Nikolai F. Rulkov (28). The Rulkov map is able to display a variety of dynamical regimes, as well as to produce irregular bursts which are observed in individual neurons through neurobiological experiments. It has been considered in a variety of studies, such as phase synchronization in clustered networks (29), suppression of burst

synchronization (30) and control of bursting synchronization (31). The Rulkov's neurons can be connected to each other by means of a random structure introduced by Erdős-Rényi (32) or of a small-world network (33, 34). In the random network, the nodes are randomly connected by means of a pre-determined connection probability. Watts and Strogatz (33) introduced small-world networks. A small-world graph exhibits a high degree of clustering as in the regular networks, where all nodes have the same number of neighbors, and also has a small average distance between the nodes as in the random networks. In the small-world networks introduced by Watts and Strogatz, non-local links are inserted by randomly rewiring some local connections into non-local ones (33), while randomly selected shortcuts are added in a regular lattice by Newman and Watts (34). In the brain, the connections between neurons are local (connections with their nearest neighbors) and non-local (long range connections) (35, 36). The topological properties of small-world ensure the efficient generation and integration of information in the brain (37). Small-world networks have been proposed to be an efficient solution for achieving phase synchronization of bursting neurons (29). It has been observed that small-world networks can exhibit synchronous behavior with fewer connections than networks with all-to-all coupling (38). Small-world properties were identified in the nematode *Caenorhabditis elegans* that has 2462 synaptic connections among each one of the 282 neurons (39).

The neurons connected to each other form a large layered neural network in which the different cortical layers have particular distributions of neural cell types, as well as have connections with other cortical and sub-cortical regions and non-cortical nuclei (40, 41). Each discrete area of the brain is described as a subnetwork exhibiting small-world properties (42), which are a high degree of clustering and a small averaged distance between vertices (nodes) (43). Subnetworks appear in the brain and they interact with each other during task accomplishing. Xu et al. (44) demonstrated that multiple cognitive processes may be related to common brain regions during cognitive tasks. Neural synchronization has been observed in the brain during different tasks (45). Jiang et al. (46) showed results in which the synchronization increases in the left inferior frontal cortex during a face-to-face dialogue. Furthermore, the combination of short path length and high clustering makes the small-world topology an attractive model for the studies about the connectivity of the nervous system (37, 47). Scannell et al. investigated the anatomical connectivity matrix of the visual cortex for the macaque monkey and the cat. They found that the values of the average path length and clustering coefficient are in accordance with expected small-world properties (48, 49). Hilgetag et al. (50) demonstrated that small-world network characteristics can be observed in cortical connectivity matrices from cat and macaque monkey brains. Moreover, there have been studies of large-scale anatomical connection patterns of the human cortex using cortical thickness measurements from magnetic resonance imaging (51). Sun et al. (52) explored burst synchronization transitions in a neural network of subnetworks. They showed the effects of intra and intercoupling strength on the burst synchronization. Lameu et al. (53) studied coupled small-world networks according to the cat cerebral cortex. They reported an emergence of bursting synchronization among neurons within the visual, somato-

sensory-motor, and frontolimbic cognitive regions, except for the auditory area. Therefore, a network of small-world networks has been used to analyze phase synchronization of bursting neurons (29).

The brain can modify its organization and function throughout the life. This ability is known as neuroplasticity and can occur in response to stimuli or injury (54). Regarding the various researches in the past century, neural plasticity is an essential feature of nervous systems in living organisms from insects to humans. The existence of changes in the brain functions was proposed by James (55) in 1890. In the late 1800s, Cajal (56) used the term plasticity to describe brain adaptation due to the environment. Alterations in neural pathways were observed in experiments performed in 1923 by Lashley (57). Hebb (58) in 1949 postulated that the synapse between two neurons is potentiated when they are active at the same time. Two decades after the Hebb's rule, experimental results about the potentiation were found in the rabbit hippocampus (59). In the context of neuroplasticity, mathematical models of networks have been considered to mimic effects of plasticity in synchronous behavior and its transition in neural networks (60). Popovych et al. (61) studied the noise dependency of synchronous behavior in a neural network model with spike-timing-dependent plasticity (STDP). Borges et al. (62–64) reported that STDP can induce non-trivial topology in the brain and that the direction of the synapses containing high and low frequency neurons changes by the STDP according to the Hebbian rules. Another type of neuroplasticity is the burst-timing-dependent plasticity (BTDP) (65), that induces synaptic alteration according to the timing of bursts. Wang et al. (66) found the coexistence of coherent and incoherent dynamics, known as chimera states, in an adaptive neural network with BTDP. They built a network of coupled two-variable integrate-and-fire model of Izhikevich. It was shown that the BTDP is able to lead static networks to different behaviors. Considering BTDP related to spontaneous retinal activity, Gjorgjieva et al. (67) performed simulations with the nonlinear integrate-and-fire model to compare results with the linear model. Recently, Silveira et al. (68) considered BTDP to analyze its effects on synchronous behavior in neural networks, such as small-world and random networks. Bursting synchronization can be induced by neuroplasticity, as well as by a Gaussian white noise applied in the plastic network.

Furthermore, external pulsed currents introduced in (69) cause alterations in neuron spiking activities, influence the bursting synchronous behavior in a neural network, and also can theoretically describe deep brain stimulation (DBS), which can be used to treat and control some neurological conditions, such as Alzheimer's and Parkinson's diseases. The DBS consists of electrodes implanted in the brain, generating electrical impulses to regulate abnormal neural activities, for instance, in patients with epilepsy. Experimental evidences have been demonstrated that pulsed current stimulation can increase cerebral plasticity and improve the locomotor function (70). Jaberzadeh et al. (71) analyzed the effects of pulsed current stimulation on corticospinal excitability. Boareto et al. (72) considered different protocols applying pulsed currents to suppress phase synchronization in scale-free neural networks. Hansen et al. (73) studied the dynamics of uncoupled and random coupled Hodgkin-Huxley neurons under periodic, ran-

dom, and mixed external perturbations. It was shown that external pulsed currents are able to change synchronous behavior of coupled neurons. Lameu et al. (53) studied coupled small-world network according to the cat cerebral cortex. Without external perturbations, they showed an emergence of bursting synchronization among neurons within the visual, somatosensory-motor, and frontolimbic cognitive regions, except for the auditory area, while burst synchronization appeared in the auditory area when some perturbations were applied in the visual area.

Given this context, this thesis aims to understand the effect of external pulsed perturbations, periodic and random pulses, on bursting neural synchronization in two different neural networks, one influenced by burst-timing-dependent plasticity (BTDP) and another one built according to the structural connectivity matrix of a healthy human brain. This objective can be divided into two independent research areas, described as:

#### Research Area 1:

- To build a neural network model containing Rulkov's neurons, which are connected to each other by means of a random structure, Erdős-Rényi model;
- To investigate the formation and destruction of bursting synchronization in the random neural network model in which the dynamics are influenced by burst-timing-dependent plasticity;
- To study the effect of two external pulsed currents on bursting synchronization in the plastic neural network.

#### Research Area II:

- To build a neural network model composed of coupled subnetworks with small-world characteristics according to one human cerebral cortex, limbic system, and brain stem;
- To study the effect of two external perturbations, periodic and random pulses, on bursting synchronization in the neural network designed in which the neurons are modelled by the Rulkov map.

The Research Area 1 and 2 have been published in *The European Physical Journal Special Topics* and in *Chaos: An Interdisciplinary Journal of Nonlinear Science*, respectively. This thesis is divided into four chapters. The first chapter is devoted to introducing all the theoretical frameworks used in this work. In Chapter 3, as Research Area 1, it is investigated the effect of burst-timing-dependent plasticity and external pulsed perturbations on bursting synchronization in the neural network containing Rulkov's neurons, which are connected to each other by means of a random structure. In Chapter 4, as Research Area 2, is studied the burst synchronization and desynchronization in a neural network model composed of 83 subnetworks available in both hemispheres of a human brain. The periodic and random pulses are applied to investigate how such perturbations influence the neural synchronization in the network. At last, the conclusions based on the results and also future perspectives are presented in Chapter 5.



## 2 BASIC CONCEPTS

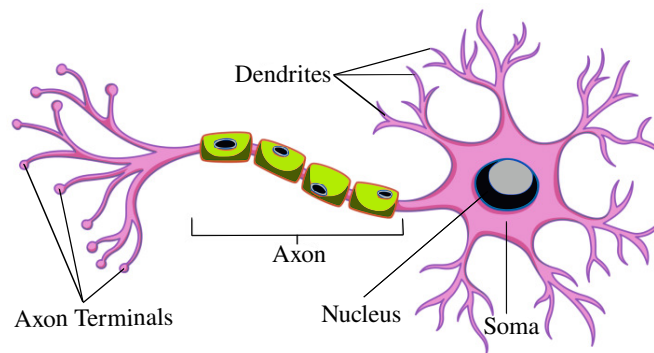
This chapter presents basic concepts related to neural network models, such as the neuron and its main components; the states of neural membrane potential, as well as the mechanisms involved in the evolution of its value; and the way in which the neurons commonly communicate, through synapses. In addition, the model proposed by Nikolai F. Rulkov (28), in which, with two discrete equations, the dynamics of the action potential observed in biological neurons can be reproduced, is described. This model is used to describe the dynamics of the neural networks of the present work. After that, it is introduced some concepts of the graph theory, which are used in the networks study. The way that the connections are distributed characterizes the network connection topology. In this thesis, all the networks were generated using a Python language package called “NetworkX” (74) which was developed for exploration and analysis of networks and network algorithms. Furthermore, it is introduced some concepts of the synchronization of dynamic systems, based on the Kuramoto oscillator model. In particular, it is considered as a powerful tool to quantify phase synchronization, called the Kuramoto order parameter, which can be generalized to measure phase synchronization of neural models (5). lastly, the external pulsed perturbations, which can be periodic or random pulses, are explained to theoretically describe deep brain stimulation (DBS), as a neurosurgical procedure.

### 2.1 NEURON, ACTION POTENTIAL AND SYNAPSES

Neurons, also called nerve cells, are the main cells of the brain and the nervous system that are responsible for receiving sensory input from the external world, for sending motor commands to our muscles and for transforming and relaying the electrical signals at every step in between (23). Although there are about 100 different types of neurons (75), each with its own anatomical and functional characteristics (76), the vast majority of neurons have the same basic structure (77). The neuron can be divided into three main parts: cell body, also known as soma, which contains the nucleus; dendrites, whose main function is the reception of signals which come from other neurons; axon, which carries the signals from the soma to other neurons and has many branches called axon terminals (16, 78, 79) (as shown in Fig. 2.1). In general, the dendrites are short, while the axon can be about one meter long (80). The cell body along with the dendrites are responsible for the reception and integration of stimuli that reaches the cell (81).

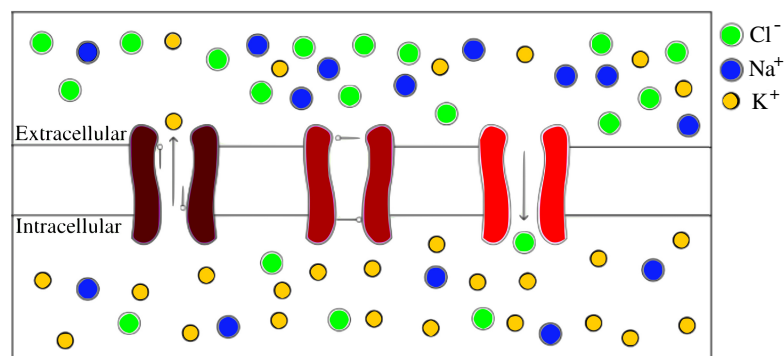
The main function of neuron is the transmission of action potentials, which are electrical signals propagating information at the nervous system. The action potential consists of a depolarization followed by repolarization, showing a spike shape. These variations at the membrane potential occur due to the variations of the ion concentrations between the intracellular and ex-

Figure 2.1: Basic anatomy of a neuron. A typical neuron can be separated into three basic regions: the soma including nucleus, dendrites and axon including axon terminals (16).



Source: Adapted from (82).

Figure 2.2: Cell membrane representation. The cell membrane contains proteins functioning as channels that allow the ions to move through it. The ion flux changes the concentration of the intracellular and extracellular sides, inducing variations in the membrane potential.



Source: The author.

tracellular media. In this sense, the membrane potential can be described as

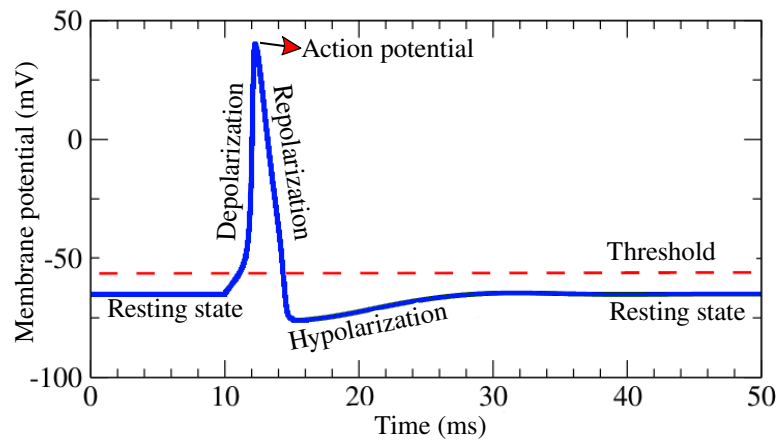
$$P(t) = P_{int} - P_{ext}, \quad (2.1)$$

where  $P_{int}$  and  $P_{ext}$  are the potentials of the intracellular and extracellular media, respectively.

The ions permeate the neural membrane by proteins working as ion channels. There are gated and non-gated ion channels. Non-gated channels are always open, allowing the entrance and exit of ions from the intracellular side, while gated channels depend on potential, meaning that the permissiveness of the channels depends directly on the potential of the membrane. The predominant ions found on both sides of the cell membrane are potassium ( $K^+$ ), sodium ( $Na^+$ ), and chlorine ( $Cl^-$ ) ions. One representation of the ionic channels is displayed in Fig. 2.2, where one channel is open allowing the exit of a  $K^+$  ion, another one is closed and a non-gated channel allows the entrance of a  $Cl^-$  ion.

At the equilibrium point, also called the resting state, there are no ionic changes between the media. In this case, the intracellular side contains in majority  $K^+$  ions, while  $Na^+$  and  $Cl^-$

Figure 2.3: Typical action potential of the neuron, identifying the resting state, depolarization, repolarization, and hyperpolarization. The threshold potential is indicated by the dashed line.



Source: Adapted from (84).

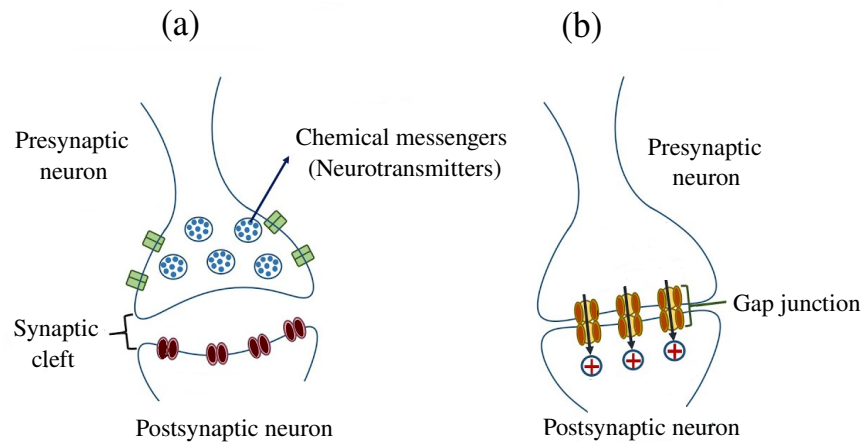
ions are more abundant in the extracellular side (83). The membrane potential is determined primarily by the  $K^+$  resting potential given as

$$P(t) = P_{int} - P_{ext} = P_{rest} \approx -70mV. \quad (2.2)$$

When the neuron is stimulated above a threshold ( $-50mV$ ), the  $Na^+$  channels allow the entrance of ions inside the cell. This influx of  $Na^+$  ions tends to depolarize the cell that results in a positive variation in  $P(t)$ . This sudden increase of  $P$  inverts the polarity of the cell, closing the  $Na^+$  ion channels and opening the  $K^+$  ion channels, to allow the efflux of  $K^+$  ions in order to repolarize the cell. This action takes the membrane potential to a level below the  $P_{res}$  and then occurs hyperpolarization. Until the  $K^+$  channels close again, the membrane is in a resistant stage. During this time, the cell exchanges excess  $Na^+$  ions inside the cell with excess  $K^+$  ions outside the cell, and the stimulus is maintained if a new cycle can be started (83). Figure 2.3 exhibits the variant states of a typical neural action potential.

The brain consists of approximately  $10^{11}$  neural cells interconnecting by  $10^{15}$  junctions called synapses to create groups of connected neurons divided into brain regions, each with specific functions (16). The synapses generally consist of three components: the axon terminals of a presynaptic neuron, a target on a postsynaptic neuron, and a connection zone between both neurons called synaptic cleft. The structure of the zone determines the type of the synapse, which can be electrical or chemical synapse (85). The synapses are responsible for carrying electrical signals initiated from the presynaptic neuron and propagated within the postsynaptic neuron through electrical and chemical synapses, as a result of the difference in electrical potential between the exterior and the interior of the neuron (16). Most synapses are chemical; these synapses communicate by means of chemical messengers, while other synapses are electrical; in these synapses, ions flow directly between cells (81). In other words, the electrical signals are

Figure 2.4: Schematic representation of the (a) chemical and (b) electrical synapses.



Source: Adapted from (86).

action potentials, which transmit the information from a neuron to the other, while the chemical signals are neurotransmitters, which transmit the information from one neuron to the next. Figure 2.4 schematically shows the (a) chemical and (b) electrical synapses.

The electrical synapses are characterized by a direct interaction among ions of the two cells, where the presynaptic axon terminal and the postsynaptic cell are very close through the regions called gap junctions. The signal produced by the action potential of the presynaptic neuron reaches the postsynaptic neuron at a gap junction connecting both neurons (16). In this sense, the postsynaptic neuron receives a synaptic current defined as

$$I_{syn} = C_{syn}(P_{pre} - P_{post}), \quad (2.3)$$

where  $C_{syn}$  represents the conductance of the channels, and  $P_{pre}$  and  $P_{post}$  are the membrane potentials of the presynaptic and postsynaptic neurons, respectively.

In the chemical synapses, the connections do not occur directly. The action potential of the presynaptic neuron releases neurotransmitters, such as glutamate and  $\gamma$ -Aminobutyric acid (GABA) in cortical neurons (83). These neurotransmitters diffuse through the synaptic cleft to reach the postsynaptic neuron through opening or closing ion channels. For these cases, the synaptic current is described by

$$I_{syn} = C_{syn}f(t)(R_{syn} - P_{post}), \quad (2.4)$$

where  $f(t)$  is a function that simulates the neurotransmitter kinetics, and  $R_{syn}$  is the reversal synaptic potential which signifies if the synapse is inhibitory or excitatory. Inhibitory synapses decrease the likelihood of a postsynaptic action potential and the neural activity, while excitatory ones increase this likelihood and the neuron activity (87). Gamma-aminobutyric acid (GABA),

glycine and serotonin are examples of inhibitory neurotransmitters, while excitatory neurotransmitters include glutamate, epinephrine and norepinephrine. A way of modeling  $f(t)$  is done by considering a sigmoidal function (83)

$$f(t) = \frac{1}{1 + \exp(-\alpha_s(P_{pre}(t) - \beta_s))}, \quad (2.5)$$

where  $\alpha_s$  and  $\beta_s$  are constants related to chemical synapses, adjusted for the respective neural model. Another way to model  $f(t)$  is with a kinetic function, which takes into account the fraction of open channels that allow the transmission of neurotransmitters,

$$\frac{df}{dt} = \left(\frac{1}{\tau_f} - \frac{1}{\tau_d}\right) \frac{1-f}{1 + \exp[-s_0(P_{pre}(t) - R_0)]} - \frac{f}{\tau_d}, \quad (2.6)$$

in which  $\tau_f$  and  $\tau_d$  are characteristic times,  $s_0 = 1/mV$  is a unitary constant, and  $R_0$  is a reversal potential (87).

## 2.2 NURON MODEL

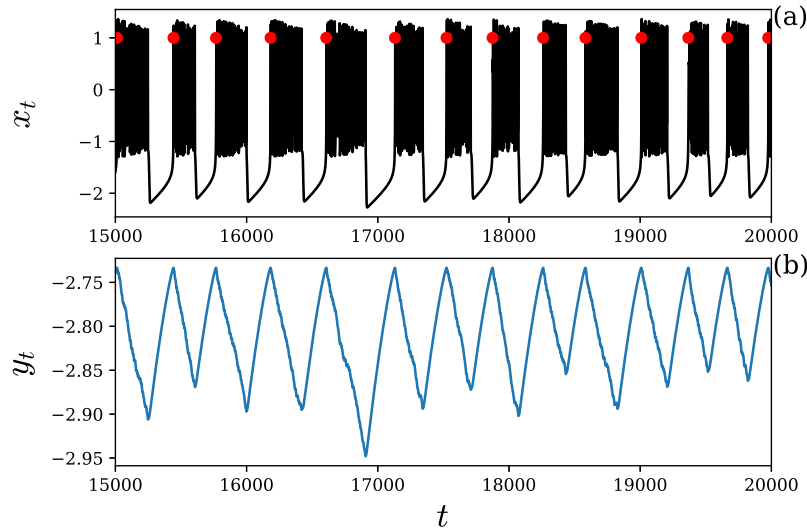
Map-based models, such as Rulkov model, have been used to mimic neural behaviors as observed in biological neurons (88). The Rulkov model is a two-dimensional iterated map that is capable of restructuring neural collective behavior and producing silent, tonic and spiking-bursting behaviors similar to those observed in individual neurons through neurobiological experiments. The low-dimensionality of this map allows to study large neural networks. Recently, the model has widely been used, due to the fact that it reduces the calculations of large neural networks and is easier and faster to compute than differential equations (73). Each node in a neural network can be described by the Rulkov map proposed by Nikolai F. Rulkov (28) in 2001. The Rulkov model containing two fast and slow variables is given by

$$x_{t+1} = \frac{\alpha}{1 + x_t^2} + y_t, \quad (2.7)$$

$$y_{t+1} = y_t - \delta(x_t - \beta), \quad (2.8)$$

where  $x_t$  represents the membrane potential of the neuron and is considered as the fast variable at the discrete time  $t$  and  $y_t$  denotes the slow variable at the discrete time  $t$ . Variable  $y_t$ , unlike variable  $x_t$ , does not have a biological meaning (28). The variables  $x_t$  and  $y_t$  are randomly selected from  $[-2, 2]$  and  $[-4, 0]$ , respectively.  $\alpha$  is a control parameter that can affect the spiking time-scale and values in that the time series of  $x_t$  presents an irregular sequence of spikes. Then, this parameter is selected in the interval  $\alpha > 4$ , due to the fact that the chaotic bursts are observed in this range. The parameters  $\delta$  and  $\beta$  describe the slow time-scale. The variable  $y_t$  is small due to the external influences of  $0 < \delta \ll 1$  and  $0 < \beta \ll 1$ . Various combinations of both  $\alpha$  and  $\beta$  can be useful to describe different dynamical behaviors of the neurons, such as resting, tonic

Figure 2.5: Time evolution of (a) the fast variable ( $x_t$ ) and (b) the slow variable ( $y_t$ ), where the red circles correspond to the bursting beginning.  $x_0$  and  $y_0$  are randomly selected from the interval  $[-2, 2]$  and  $[-4, 0]$ , respectively,  $\alpha = 4.1$ ,  $\delta = 0.001$ , and  $\beta = 0.001$ .



Source: The author.

spiking, and chaotic bursts. The time series of the fast and slow variables and the maximum values of the slow variable are displayed in Fig. 2.5.

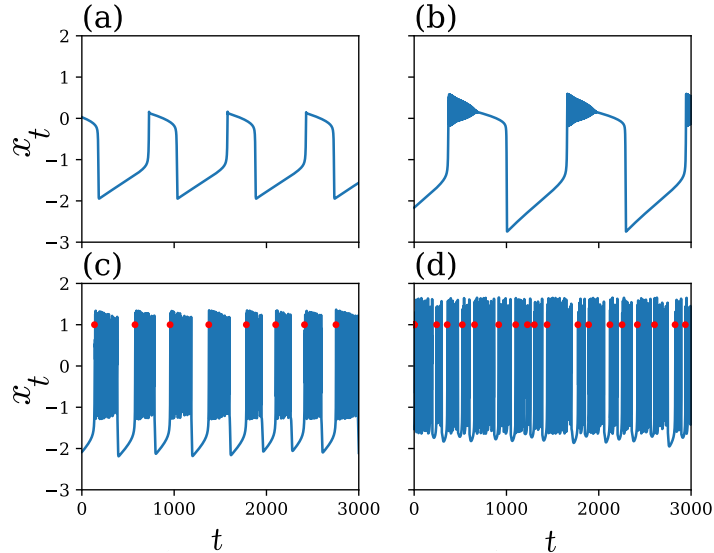
Figures 2.6(a) and 2.6(b) display the regimes of relaxation oscillations and pieces of spikes with amplitude decreasing, respectively. In Figs. 2.6(c) and 2.6(d), the Rulkov map exhibits bursting behavior and the red circles denote the maximum value of the slow variable  $y_k$ . The chaotic bursts are observed for  $\alpha > 4$ .

### 2.3 GRAPH THEORY AND COMPLEX NETWORKS

The graph theory developed in part by Leonard Euler (89) is a section of discrete mathematics to solve the challenge of the Königsberg bridges. When passing through the city of Königsberg, the Pregel River creates two islands connected to the city by seven bridges. The challenge, regardless of where the journey started or ended, was to cross all the bridges without repeating. Figure 2.7 illustrates one adaptation of the original illustration of the challenge made by Euler (90). To solve this challenge, the idea was to represent each area and the bridges as sites linked by edges. Since all the regions had an odd number of bridges, therefore, there was no solution for this challenge. To solve it, it was necessary to remove each of the bridges. The way in that Euler obtained his results was considered as a starting point for the study of graph theory (91).

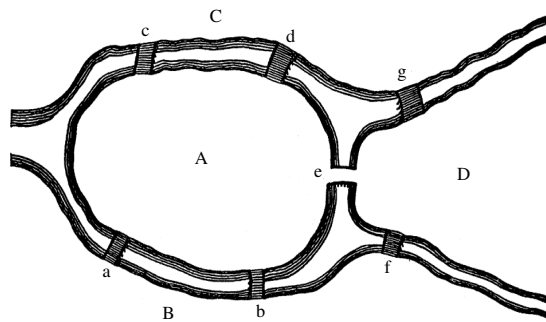
A graph  $G$  consists of a finite set of nodes (or vertices),  $N$ , connected by links called edges (or connections),  $E$ , (90).  $N$  is a non-empty discrete set of nodes, and  $E$  is a subset constituted of ordered pair of  $N$  elements. For two nodes, the pair  $(n_i, n_j) \in E$  is a line which connects

Figure 2.6: Time evolution of the fast variable  $x_k$  for (a)  $\alpha = 2.3$ , (b)  $\alpha = 3.0$ , (c)  $\alpha = 4.1$ , and (d)  $\alpha = 4.5$ . The red circles show the maximum value of the slow variable  $y_k$ .  $x_0$  and  $y_0$  are randomly selected from the interval  $[-2, 2]$  and  $[-4, 0]$ , respectively,  $\delta = 0.001$  and  $\beta = 0.001$ .



Source: The author.

Figure 2.7: Illustration of the Königsberg bridges. The Pregel River ramifications form two islands  $A$  and  $D$ , which are connected to the city by the 7 bridges  $a, b, c, d, e, f$ , and  $g$ .



Source: Adapted from (89).

the neurons  $n_i$  and  $n_j$ . The connections between nodes can be binary or weighted: for a binary connection, if the nodes are connected,  $(n_i, n_j) = 1$ ; or otherwise 0 for a weighted one, when some connections are more relevant than others. On the other hand, the connections can be directed and non-directed: in a non-directed connection, the connections are reciprocal which means that, if  $n_i$  is connected to  $n_j$ , it implies that  $n_j$  is connected to  $n_i$ ; in a directed one, the connections are not reciprocal. The notation  $G(N, E)$  represents a graph with  $N$  nodes and  $E$  connections. The graph  $G$  can be represented as a squared matrix,  $N \times N$ , also known as a connection matrix, where  $N$  is the number of rows and columns, and  $E$  is the number of non-zero elements. In the matrix, zero and non-zero elements indicate the absence and presence of a relationship between the nodes of a network, respectively.

The graph theory can be used in the study of networks, in particular, neural networks, by considering each node of the network as a neuron and their connections as the synapses. The global behavior of a group of connected entities is studied by means of a complex network. The network topology that plays a key role in the global dynamics of the network depends on how the connections are distributed in the network (92). In this sense, the topology of the network containing  $N$  as the size of the network and  $E$  as the number of connections is classified using some topological measurements, such as average shortest path length and clustering coefficient.

The average shortest path length, ASPL, also known as average path length, as a concept in the network topology is described by the average number of edges along the shortest paths for all possible pairs of nodes in the graph (93). It measures the efficiency of information or mass transport on a graph. The average path length as a measure of the average number of edges transmitted from one node to another in the network is defined by

$$ASPL = \frac{1}{N(N-1)} \sum_{i=1}^N \sum_{j=1}^N d(n_i, n_j), \quad (2.9)$$

where  $d(n_i, n_j)$  denotes the shortest distance between two nodes  $n_i$  and  $n_j$ , and  $N$  is the number of nodes.

The clustering coefficient, CC, measures the degree indicating the tendency of nodes in a graph to cluster together (94). When the graph is more complete, meaning that the connections are dense, the clustering coefficient is high. In fact, it is a sign of triadic closure because the more complete the graph is, the more triangles will usually arise (95). Then, the clustering coefficient  $CC$  for each node  $i$ ,  $CC(i)$ , is defined by

$$CC(i) = \frac{2k(i)}{m(i)(m(i)-1)}, \quad (2.10)$$

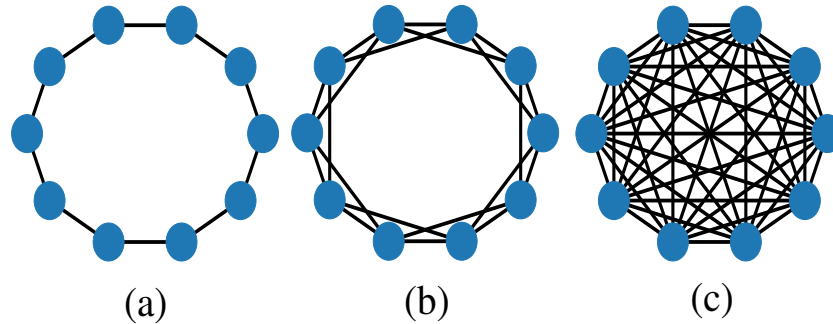
where  $k(i)$  and  $m(i)$  represent the number of edges among the neighbors of node  $i$  and the degree of node  $i$ , respectively. In fact, clustering coefficient gives a measure of modularity of the network. When the clustering coefficient is 1, it means that the neighborhood of the node is fully connected and a value close to 0, when there are almost no connections in the neighborhood.

Some graph generators, such as regular, random (without structure), and small-world network models, to describe different network topologies are explained as follows. A regular network is the simplest network topology in which all the nodes have the same number of neighbors as edges, meaning that the  $i$ -th node is connected to its closest neighbors. Figure 2.8 shows an example of the three regular networks with  $N = 10$  nodes.

Another topology is the random network topology, where the nodes are randomly connected by means of a pre-determined connection probability (96). One of the possibilities to build such network is using the Erdős-Rényi algorithm (32) in which a connection probability ( $p_r$ ) between 0 and 1 ( $0 \leq p_r \leq 1$ ) is considered. In the network, the number of connections is estimated by  $E_r = p_r N(N-1)$ . The random graph has low clustering and short path length.

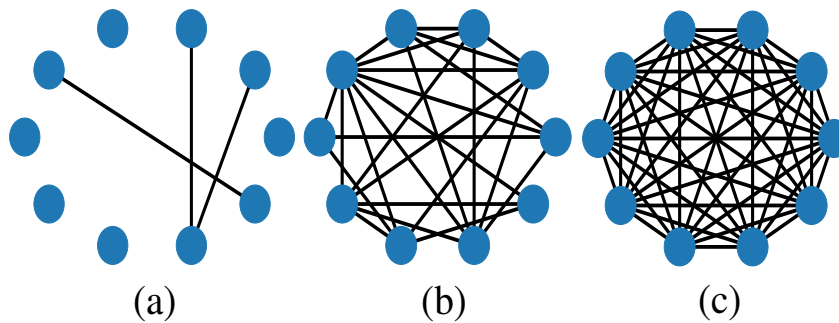


Figure 2.8: Examples of regular graphs for 10 nodes linked to their (a) 2 nearest neighbors, (b) 4 nearest neighbors and (c) all the possible neighbors to form a global network (complete network).



Source: The author.

Figure 2.9: Examples of random graphs for 10 nodes with (a)  $p_r = 0.05$ , (b)  $p_r = 0.5$  and (c)  $p_r = 1$ .



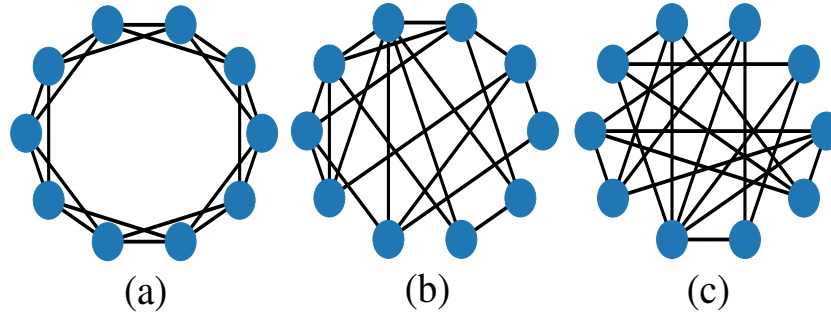
Source: The author.

Figure 2.9 illustrates examples of random networks with  $N = 10$  and (a)  $p_r = 0.05$ , that in this case the small number of connections makes possible to find some parts separated from the network, (b)  $p_r = 0.5$  and (c)  $p_r = 1$  for all the possible connections.

Although the regular and random network topologies are idealization cases, it is believed that real networks are between these extremes of order and randomness (92). In 1998, Watts and Strogatz demonstrated that a network with shortcuts can exhibit average shortest path length as in the random networks and high clustering coefficient as in the regular networks. These networks were called small-world networks (33). A small-world network consists of nodes that most of them are not neighbors of one another, but the neighbors of any given node are likely to be neighbors of each other. Most nodes can be accessed from every other node with a small number of hops or steps. It was found that some real networks have the same topological characteristics of a small-world network, such as the worldwide-web (97–99), electric power grids (97) and even neural networks, like the nematode nervous system *C. Elegans* (33,97) and in the anatomy of the mammal brains (37).

One of the ways to generate a small-world network is using the Watts-Strogatz algorithm (33). First, a regular network is built with  $N$  nodes and  $E_0$  connections. After that,  $E_{ws}$  con-

Figure 2.10: Examples of Watts-Strogatz graphs for 10 nodes linked to their 4 nearest neighbors with (a)  $p_{ws} = 0$  as a regular network, (b)  $p_{ws} = 0.5$  as a small-world network and (c)  $p_{ws} = 1$  as a random network. The small-world regime is achieved between the extremes of order and randomness.



Source: The author.

nections are randomly replaced, as the number of connections  $E_{ws}$  is controlled by a probability  $p_{ws}$ , where  $E_{ws} = p_{ws}E_0$ . When  $p_{ws} \approx 0$ , the network shows the same features of a regular one and when  $p_{ws} \approx 1$ , the network has the same characteristics of a random one, however, when  $p_{ws}$  is quantified by intermediate values, the number of shortcuts can put the network in the small-world regime, presenting a high cluster coefficient and low average shortest path length. Figure 2.10 illustrates an example of Watts-Strogatz graph with 10 nodes linked to their 4 nearest neighbors for (a)  $p_{ws} = 0$ , (b)  $p_{ws} = 0.5$  and (c)  $p_{ws} = 1$ .

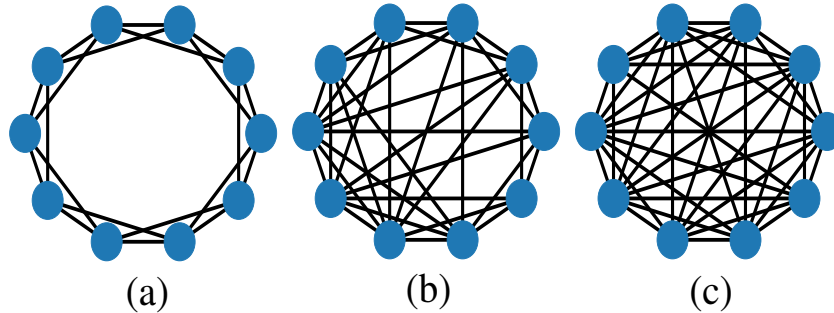
However, in the Watts-Strogatz small-world networks, since non-local links are inserted by randomly rewiring some local connections into non-local ones (33), it is possible to disconnect a neuron from the network. To avoid this, Newmann and Watts proposed an alternative algorithm to achieve the small-world regime. In the Newmann and Watts small-world network, randomly selected shortcuts are added in a regular lattice instead of replacing them (34). For this network, the number of connections depends on a probability  $p_{nw}$ . If the number of connections of the regular network is  $E_0$ , the new number of connections is described by  $E_{nw} = (1 + p_{nw})E_0$ , meaning that for each existing connection ( $E_0$ ), a new random connection can be added with a probability  $p_{nw}$  (98, 100). Figure 2.11 displays an example of Newman-Watts network with 10 nodes connected to their 4 nearest neighbors for (a)  $p_{ws} = 0$ , (b)  $p_{ws} = 0.5$  and (c)  $p_{ws} = 1$ , forming a network which is no longer in the small-world regime.

In general, in the Watts-Strogatz small-world networks, some local connections are replaced by non-local connections, while all the local connections exist in the Newmann-Watts small-world networks.

## 2.4 PHASE SYNCHRONIZATION

Synchronization, as a basic nonlinear phenomena, was detected when the scientist Christiaan Huygens, in the 17th century, reported his observations where two very weakly coupled pendulum clocks are synchronized in-phase (2). In the context of dynamic systems, there have been

Figure 2.11: Examples of Newman-Watts graphs for 10 nodes connected to their 4 nearest neighbors with (a)  $p_{ws} = 0$  as a regular network, (b)  $p_{ws} = 0.5$  as a small-world network and (c)  $p_{ws} = 1$  as a network that is no longer in the small-world regime.



Source: The author.

many variant synchronization states. Complete (or identical) synchronization, as the simplest form of synchronization, consists of the precise convergence of all the system paths to a unique synchronization. Frequency synchronization consists of the frequency, which locks the system in which all elements of the system evolve with the same periodicity. Phase synchronization that was beyond the frequencies, in which the phases are also locked (101). It is possible to describe some concepts of the synchronization of dynamic systems by means of the Kuramoto oscillator model.

The Kuramoto model is composed of an ensemble of  $N$  oscillators with a nonlinear coupling where the phase of the  $i$ -th oscillator evolving as

$$\dot{\theta}_i = \eta_i + \frac{\gamma}{N} \sum_{j=1}^N \sin(\theta_j - \theta_i), i = 1, 2, \dots, N, \quad (2.11)$$

where  $\eta_i$  is the natural frequency of the oscillator and  $\gamma$  represents the coupling strength. When  $\gamma = 0$ , each oscillator linearly evolves with its own frequency  $\theta_i(t) = \eta_i t + \theta_i(0)$ , where  $\theta_i(0)$  indicates the initial condition of the  $i$ -th oscillator.

For the particular case of identical oscillators  $\eta_i = \eta_0, \forall i$ , and, without losing generality  $\eta_0 = 0$  (it is always possible to select a frame rotating at the same frequency  $\eta_0$  when  $\eta_0 \neq 0$ ), then

$$\dot{\theta}_i = \frac{\gamma}{N} \sum_{j=1}^N \sin(\theta_j - \theta_i), i = 1, 2, \dots, N. \quad (2.12)$$

Considering a vector  $\theta = (\theta_1, \theta_2, \dots, \theta_N)$ , it is shown that Eq. 2.12 exhibits a gradient equation  $\dot{\theta} = -\nabla U$  (102), where the potential function is defined by

$$P = -\frac{\gamma}{2N} \sum_{i=1}^N \sum_{j=1}^N \cos(\theta_j - \theta_i). \quad (2.13)$$

It means that the trajectories of such systems monotonically flow at the potential surface and

asymptotically approach the equilibrium point  $\dot{\theta} = 0$ . When  $\gamma > 0$ , some symmetric initial conditions around the circle  $[0, 2\pi]$  lead the system to a steady-state solution, called twisted states (102), due to the fact that the sinusoidal sum between all oscillators mutually is cancelled. When non-symmetric initial conditions are considered, the coupling leads the system to a phase-locking stable state, where  $\theta_1 = \theta_2 = \dots = \theta_N$ , called complete phase synchronized state.

For non-identical oscillators, the natural frequency of the oscillators can be described based on a probability density  $h(\eta)$ , which is considered as a function of a mean frequency  $\Omega$ ,

$$h(\Omega - \eta) = h(\Omega + \eta). \quad (2.14)$$

Kuramoto defined a complex mean-field  $Z$ , which is described as

$$Z = R(t)e^{i\psi(t)} = \frac{1}{N} \sum_{j=1}^N e^{i\theta_j(t)}, \quad (2.15)$$

where  $\psi$  indicates the circular average frequency. The absolute value of  $Z$ , called Kuramoto order parameter  $R$ , signifies the degree of phase coherence in the oscillators and can be used as an indicator of phase synchronization. When  $N \rightarrow \infty$ , the phase transition from the non-synchronized state to the phase-synchronized one is observed in a critical value  $\eta^*$ , that is given by

$$\eta^* = \frac{2}{\pi h(0)}, \quad (2.16)$$

and the modulus of the Kuramoto order parameter is determined by

$$R = \begin{cases} 0, & \text{for } \eta \leq \eta^* \\ \sqrt{\frac{-16}{\pi(\eta^*)^3 h''(0)} \left(1 - \frac{\eta^*}{\eta}\right)}, & \text{for } \eta > \eta^*. \end{cases} \quad (2.17)$$

It means that, when  $\eta$  is lower than a critical value  $\eta^*$ , desynchronization occurs,  $R \approx 0$ , and when  $\eta > \eta^*$ ,  $R(\eta)$  asymptotically becomes equal to 1, and is equal to 1 at the limit of  $\eta \rightarrow \infty$ .

Although the order parameter was created to calculate the phase synchronization of Kuramoto oscillators, it can be effectively applied to distinct oscillators and also neurons regardless of periodicity presence. To do this, it is necessary to add a phase to the dynamic model. The phase can be obtained with a projection of the dynamic system  $\theta(t) = f(X)$  and also with the definition of an appropriate Poincare section where the orbit crosses once for each  $2\pi$  rotation. Therefore, the phase can be described as

$$\theta_i(t) = 2\pi n_i + 2\pi \frac{t - t_{n,i}}{t_{n+1,i} - t_{n,i}}, t_{n,i} \leq t < t_{n+1,i}, \quad (2.18)$$

where  $t_{n,i}$  represents the  $n$ -th time where the  $i$ -th system crosses the Poincare surface. Then, for each  $t = t_n$ , the second term of the equation vanishes and the phase is equal to  $2\pi n_i$ , for the other

instants of time, the second term interpolates these times until the next cross occurs in  $t = t_{n+1}$ . The phase increases by a factor of  $2\pi$  every  $t_{n+1,i} - t_{n,i}$  (103). After that, it is possible to quantify the phase synchronization of the system using Eq. 2.15 for the order parameter. A dynamic system might not present a stationary state of  $R(t) = R$  that is different from the Kuramoto model. To measure phase synchronization in distinct models, the average order parameter, which consists of the temporal average of the order parameter module, is described as

$$\bar{R} = \frac{1}{t_{Final} - t_{Initial}} \sum_{t=t_{Initial}}^{t_{Final}} R(t), \quad (2.19)$$

where  $t_{Initial}$  and  $t_{Final}$  are the start and end times of the order parameter computation, respectively.  $\bar{R} = 1$  corresponds to a completely phase-synchronized state, in which all elements start to cross the surface at the same time. On the other hand,  $\bar{R} = 0$  means that each element in the network has a corresponding pair that is completely out-of-phase. This is related to a completely incoherent state (completely unsynchronized) or a state with clusters of in-phase neurons that are anti-phase between themselves (104).

Throughout this thesis, it is focused on the burst phase synchronization as a type of neural synchronization, that is obtained by the maximum value of the slow variable  $y_i$  as the beginning point of bursting. It is possible to observe bursts and oscillatory patterns when the slow and fast oscillations illustrated in Fig. 2.5 are considered. The neuron's phase changes in the interval  $[0, 2\pi]$  during the evolution of  $t$ . To analyze the burst synchronization of a network, each neuron's phase at time  $t$  ( $\theta_t^i$ ) is written as

$$\theta_t^i = 2\pi n + 2\pi \frac{t - t_n^i}{t_{n+1}^i - t_n^i}, \quad (2.20)$$

where  $n$  as the first burst, is labelled by the index  $n = 0$ , describes an integer,  $t_n^i$  determines the beginning time of the  $n$ -th burst of the  $i$ -th neuron, and  $t$  is chosen from  $t_n^i$  to  $t_{n+1}^i$ . Therefore,  $t_{n+1}^i - t_n^i$  is measured as the duration of the burst that fluctuates according to  $x_t^i$  in an irregular behavior.

The phase synchronization related to bursts of neural ensemble is used to calculate the Kuramoto order parameter (105) that is essential to understand the bursting synchronous behavior of the network. The order parameter is defined by

$$R_t = \left| \frac{1}{N} \sum_{i=1}^N \exp(r\theta_t^i) \right|, \quad (2.21)$$

where  $N$  is the number of neurons and  $r$  as the imaginary unit is equal to  $\sqrt{-1}$ .  $\theta_t^i$  is the neuron's

phase  $i$  at time  $t$ . The time-averaged order parameter is given by

$$\bar{R} = \frac{1}{T} \sum_{t=t_{\text{Initial}}}^{t_{\text{Final}}} R_t, \quad (2.22)$$

where the time interval  $T$  represents the total simulation time, after a transient time and changes in the interval  $[t_{\text{Initial}}, t_{\text{Final}}]$ . If the neurons are phase-synchronized or desynchronized, the time-averaged order parameter  $\bar{R}$  is equal to 1 or 0, respectively.

If there are subnetworks in the network, as observed in the research area 2, the Kuramoto order parameter is calculated by

$$R_t = \left| \frac{1}{N \times P} \sum_{i=1}^N \sum_{p=1}^P e^{r\theta_i^{(i,p)}} \right|, \quad (2.23)$$

where  $N$  is the total number of neurons of each subnetwork,  $P$  is the number of cortical areas, and  $\theta_i^{(i,p)}$  is the phase of the neuron  $i$  in the cortical area  $p$  at time  $t$ . Eqs. 2.20 and 2.22 remain the same for this network including subnetworks.

## 2.5 EXTERNAL PULSED PERTURBATIONS

External perturbations have an important implication in the context of neural dynamics, due to the fact that perturbations can be associated with stimulus on the sensory perceptions, promoting changes in the individual or collective behavior of the neurons (106). These perturbations are associated with the external currents that can be distributed in a probabilistic way by a function (107), or can be pulsed (73). The pulses can be periodic or random. The neurons in a neural network can be stimulated by an external current which has a constant or pulsed profile.

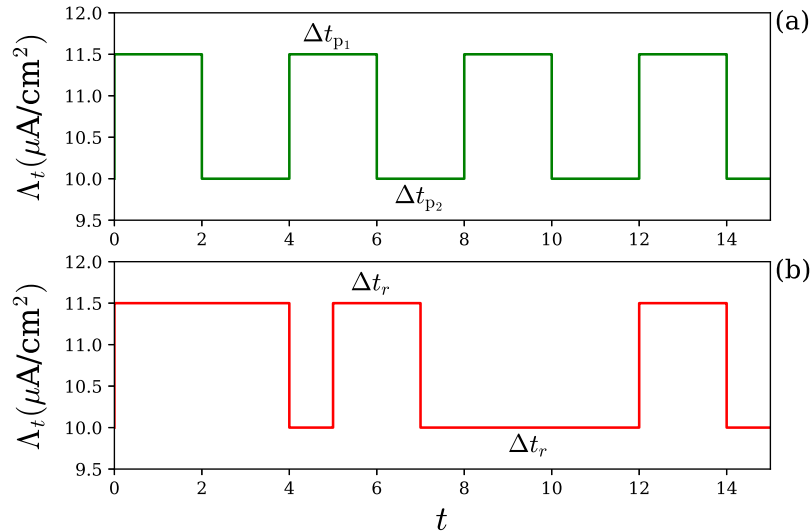
An external pulsed current, periodic or random, at time  $t$  ( $\Lambda_t$ ) for each neuron  $i$  is given by

$$\Lambda_t^i = I_0 + \psi(t), \quad (2.24)$$

where  $I_0$  represents a current with constant amplitude in  $\mu\text{A}/\text{cm}^2$  and  $\psi(t)$  describes the pulses with amplitude  $\tau$ , that can be added to  $I_0$  during a time. When the external current is pulsed,  $\psi(t)$  is assumed a value equal to 0 or  $\tau$  in an on-off configuration along time. Figure 2.12 displays a schematic representation of external currents. The first case (Fig. 2.12(a)) is a periodic pulsed current, in which the on-off transition in  $\psi(t)$  during the simulation occurs in the fixed time intervals  $\Delta t_{p_1}$  and  $\Delta t_{p_2}$ , respectively, while the second one (Fig. 2.12(b)) is a pulse in which the transition on-off in  $\psi(t)$  has time interval,  $\Delta t_r$ , randomly distributed (random uniform distribution).

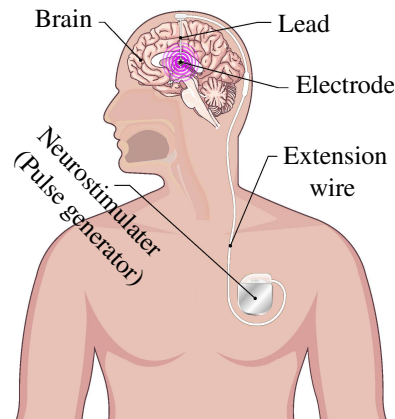
Furthermore, external pulsed currents have been used to theoretically describe deep brain stimulation (DBS) (as shown in Fig. 2.13), as a neurosurgical procedure (69). The DBS consists of electrodes implanted within certain areas of the brain, generating electrical impulses to

Figure 2.12: (a) Periodic pulsed current for  $I_0 = 10 \mu\text{A}/\text{cm}^2$ ,  $\tau = 1.5 \mu\text{A}/\text{cm}^2$ ,  $\Delta t_{p1} = 2 \text{ ms}$ , and  $\Delta t_{p2} = 2 \text{ ms}$ , and (b) random pulsed perturbation for  $I_0 = 10 \mu\text{A}/\text{cm}^2$ ,  $\tau = 1.5 \mu\text{A}/\text{cm}^2$ , and  $\Delta t_r$  randomly distributed in the interval  $[0, 20] \text{ ms}$ .



Source: The author.

Figure 2.13: The Deep Brain Stimulation system consists of three components: the lead, the extension wire, and the neurostimulator.



Source: Adapted from (110).

regulate abnormal neural activities, for instance, in patients with epilepsy, and Alzheimer's disease and to provide remarkable therapeutic benefits for otherwise treatment-resistant movement disorders such as Parkinson's disease, tremor and dystonia (108, 109). For example, movement-related symptoms of Parkinson's disease and other neurological conditions are caused by disorganized electrical signals in the areas of the brain that control movement. Therefore, the DBS interrupts the irregular signals that cause tremors and other movement symptoms. The Food and

Drug Administration (FDA) approved DBS as a treatment for essential tremor in 1997, Parkinson's disease in 2002, and dystonia in 2003 (109).

The DBS system consists of three components: the lead, the extension wire and the implanted pulse generator (neurostimulator). The lead, also called an electrode, is a thin, insulated wire that is inserted through a small opening in the skull and implanted in the brain. The tip of the electrode is positioned within the targeted brain area. The extension wire is an insulated wire that is passed under the skin of the head, neck, and shoulder, connecting the lead to the neurostimulator. The neurostimulator (the battery pack) is the third component and is usually implanted under the skin near the collarbone. The whole system lies under the skin and controls the amount of stimulation. The pacemaker device delivers a constant fast-frequency stimulus to the tip of the electrode implanted in the brain. This stimulus interrupts a specific circuit in the brain that is overactive in the disease state. This interruption of the diseased overactive circuit can significantly improve the symptoms of the disease.



### 3 RESEARCH AREA 1

Throughout the life of every individual, the brain can be altered and adapted due to neuroplasticity (54). Neuroplasticity, also known as brain plasticity or neural plasticity, allows the brain to improve its connections or rewire itself. Functional and structural plasticities are responsible for the ability to move functions from an injured area of the brain to other undamaged ones and to alter its physical organization as a result of learning, respectively (111). In other words, the synaptic modifications can help the brain to enhance fitness, to promote existing cognitive capabilities, and to recover from some brain injuries. Furthermore, brain plasticity has impacts on neural synchronization. This chapter is devoted to build a neural network composed of coupled Rulkov neurons with chemical excitatory connections randomly distributed, which are quantified with initial weight values and updated by the time difference between the burst-start points related to presynaptic and postsynaptic neurons, namely burst-timing-dependent plasticity (BTDP). After that, it is investigated the effects of external perturbations, such as periodic and random pulses, on the neural synchronous behavior of the network influenced by the BTDP rule. It is shown that the plasticity changes the synaptic weights between the presynaptic and postsynaptic neurons, and as a consequence the burst synchronization, as well as the external periodic and random pulsed perturbations can induce synchronization and desynchronization states in the plastic network.

#### 3.1 RANDOM NETWORK OF RULKOV'S NEURONS

A random neural network, containing 1000 Rulkov's neurons connected by means of a pre-determined probability distribution  $p = 0.35$  according to the Erdős-Rényi model, is built. The dynamic behavior of the neural network containing chemical excitatory synapses and external pulsed perturbation is defined by

$$x_{t+1}^i = \frac{\alpha^i}{1 + (x_t^i)^2} + y_t^i - \frac{1}{(1/N) \sum_{ij}^J C_{ij}} (x_t^i - R_s) \sum_{j=1}^J C_{ij} W_{ij,t} H(x_t^j - \varphi) + \Lambda_t^i, \quad (3.1)$$

$$y_{t+1}^i = y_t^i - \delta(x_t^i - \beta), \quad (3.2)$$

where  $x_t^i$  and  $y_t^i$  related to the neuron  $i$  at time  $t$  are randomly selected from the interval  $[-2, 2]$  and  $[-4, 0]$ , respectively.  $\alpha^i$  is randomly distributed in the interval  $[4.1, 4.4]$ ,  $\delta = 0.0009$  and  $\beta = 0.0011$ .  $N$  is the number of neurons connected to each other.  $C_{ij}$  describes the connection between the presynaptic  $i$  and postsynaptic  $j$  neurons. When the element of an adjacency matrix is equal to 1, the connection exists and 0 otherwise.  $R_s = 1$  is the reversal potential and  $H(x)$  is the Heaviside step function with the spiking threshold of the membrane potential  $\varphi$  equal to

0. Furthermore,  $\Lambda_t^i$  is an external pulsed perturbation applied in the neural network to active spikes in neurons as explained in Eq. 2.24.  $W_{ij,t}$  represents the synaptic weight of the synapse  $j \rightarrow i$  at time  $t$  and controls how strong or weak the connections are. This parameter assumes values between 0 and  $W_{\max}$  and can change over time following the plasticity rule. For the random network,  $W_{\max}$  is equal to 0.1. To quantify the synaptic weights with initial weight values and modify them as the network evolves, the burst-timing-dependent plasticity (BTDP) rule introduced by Butts et al. (65), which measures the time difference between the burst-start times (or burst latency) of two connected neurons to determine the synaptic weight change according to the equation given by

$$\Delta W(\Delta t) = \begin{cases} A_m - \frac{A_m - A_n}{T_s} |\Delta t|, & \text{if } |\Delta t| \leq T_s \\ A_n, & \text{if } |\Delta t| > T_s, \end{cases} \quad (3.3)$$

where  $A_m = 0.008$ ,  $A_n = -0.0032$ , and  $T_s = 58$ . The change in the synaptic weight is calculated with  $\Delta t$  equal to the difference between the last burst-start time of the presynaptic and postsynaptic neurons.

All synapses are updated twice for burst pair ( $W_{ij}$  is updated both when  $i$  starts a burst and when  $j$  does). To correct this,  $A_n \rightarrow N = A_n/2$  and  $A_m \rightarrow M = A_m + N$  in Eq. 3.3 are changed. In addition, the values of the synaptic weights in the range  $0 \leq W_{ij} \leq W_{\max}$  are limited. If the application of the plasticity rule results in a negative synaptic weight, or one greater than  $W_{\max}$ , the synaptic weight value is set to the trespassed limit. If both neurons burst at similar times, then the potentiation occurs, by the other hand, if the difference time between the burst-start events is large enough, the potentiation suffers a depression. A plot of the BTDP function is shown in Fig. 3.1.

The initial value for all synapses is the same synaptic weight  $W_0$ . After a transient of  $t_{trans} = 5 \times 10^4$  steps in which the neurons are active but the plasticity is not computed, the network is let to evolve for  $1 \times 10^6$  steps. During this time interval, the synaptic weights vary according to the plasticity rule, and the network synchronization level is measured.

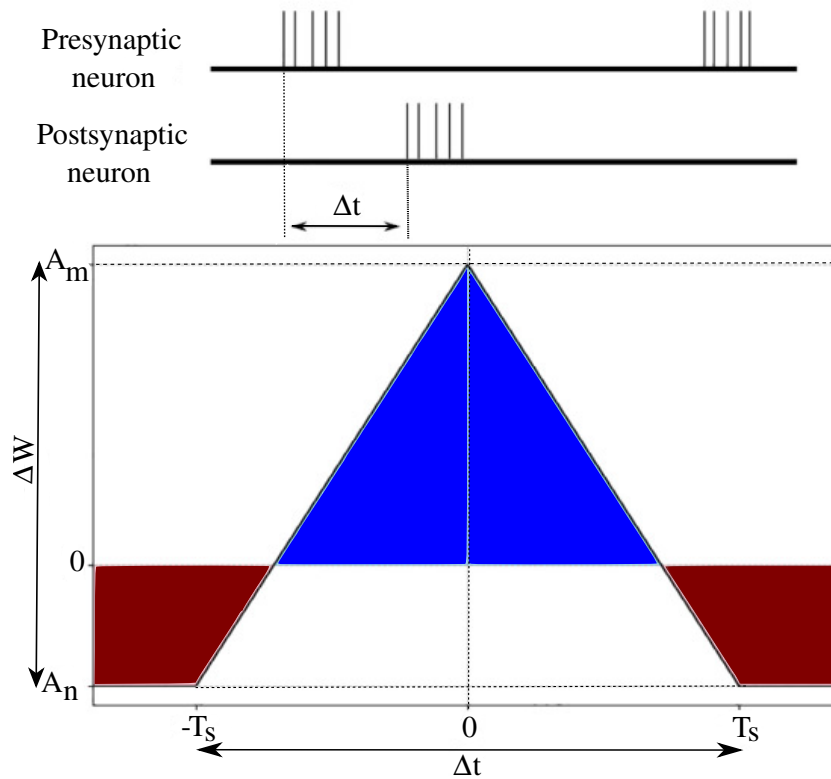
## 3.2 RESULTS

### 3.2.1 Bursting Synchronization Induced by Burst-Timing-Dependent Plasticity (BTDP)

The effects of the BTDP rule on the random neural network in terms of the order parameter in Eq. (2.21), the time-averaged order parameter in Eq. (2.22) and the mean synaptic weight in Eq. (3.4) are studied. The mean synaptic weight is defined by

$$\langle W \rangle = \frac{1}{\sum_{i,j=1}^J C_{ij}} \sum_{i,j=1}^J C_{ij} W_{ij}, \quad (3.4)$$

Figure 3.1: Change on synaptic weight as a function of the time latency between the burst-start events of two connected neurons. Bursts starting close together cause synapse potentiation, while large burst latency causes depression.



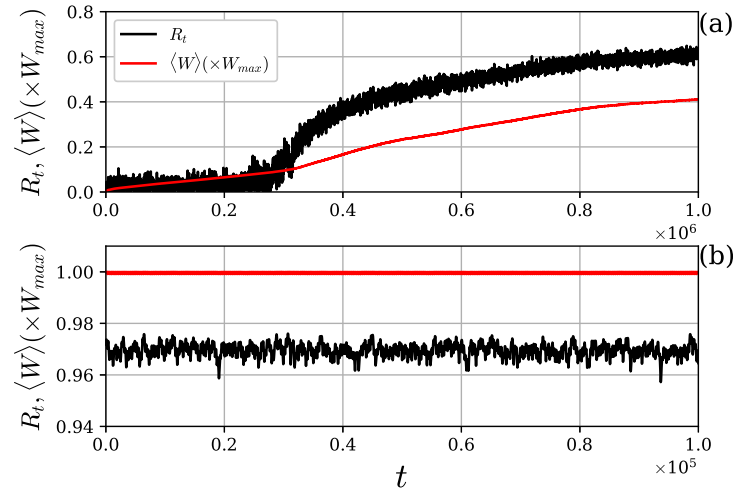
Source: Adapted from (68).

where  $\sum_{i,j=1}^J C_{ij}$  is the total number of synapses in the network.

The relation between the potentiation and burst synchronization for different initial weights is analyzed. Figure 3.2(a) displays the time series of the mean synaptic weight and the order parameter for the initial weight  $W_0 = 0$ , while the time series for  $W_0 = 0.1$  is exhibited in Fig. 3.2(b). It is verified that the potentiation starts before occurring bursting synchronization. With regard to Fig. 3.2(a) for  $W_0 = 0$  and  $t$  less than  $3 \times 10^5$  ms, the bursts of high-frequency neurons occur and the average synaptic weight slowly increases. In this case, the connections between the neurons are not strong enough and as a consequence the order parameter does not enhance. For  $t > 3 \times 10^5$  ms, the synapses become strong and the order parameter quickly increases to reach approximately 0.6 at the final time point, where the synapses are in the maximum weight value. For  $W_0 = 0.1$  (Fig. 3.2(b)), the mean synaptic weight is 0.1 and the synchronization saturates.

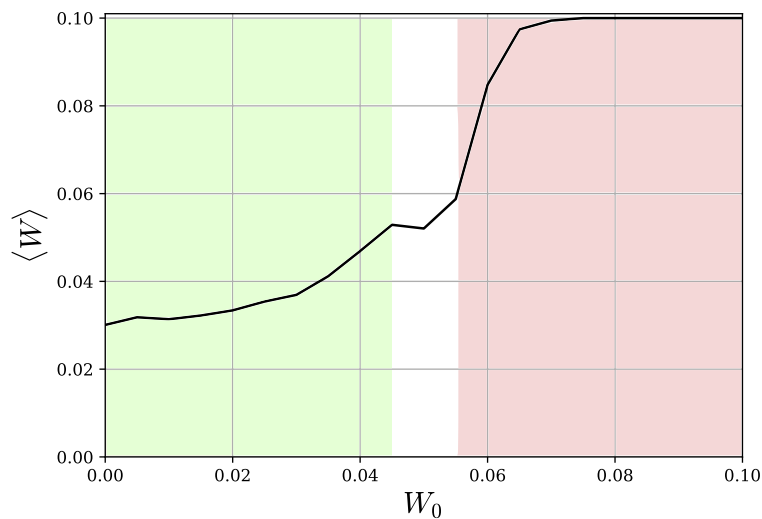
Figure 3.3 shows the average synaptic weight  $\langle W \rangle$  as a function of the initial synaptic weight value  $W_0 \in [0, 0.1]$  for the random neural network. The curves related to  $W_0 \leq 0.045$  and  $W_0 \geq 0.055$  are smooth and are connected to each other by a region in the interval  $0.045 < W_0 < 0.055$ . The occurrence of potentiation in these two parts separated from each other depends on the presence of initial synchronization in the network. The coincidence of bursts of high-frequency

Figure 3.2: Time evolution of the mean synaptic weight (red line) and order parameter (black line) for (a)  $W_0 = 0$  and (b)  $W_0 = 0.1$ . It is observed that the potentiation begins before occurring bursting synchronization.



Source: The author.

Figure 3.3: Mean synaptic weight as a function of the initial synaptic weight. The curve is separated into three parts:  $W_0 \leq 0.045$ ,  $0.045 < W_0 < 0.055$ , and  $W_0 \geq 0.055$ . The potentiation is preferred more than depression.

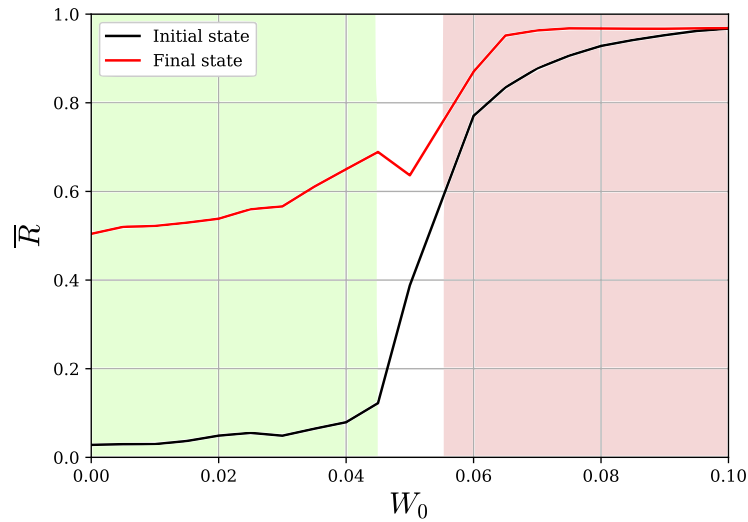


Source: The author.

neurons induces the potentiation for small  $W_0$  compared to the potentiation due to the beginning of the synchronization for large  $W_0$ . The mean synaptic weights change according to their initial synaptic weights. Therefore, the potentiation is preferred more than depression.

The time-averaged order parameter as a function of the initial synaptic weight value for

Figure 3.4: Time-averaged Kuramoto order parameter as a function of the initial synaptic weight value for before (initial state in black line) and after (final state in red line) applying the BTDP rule.



Source: The author.

before (black line) and after (red line) applying the BTDP rule to the neurons coupled is exhibited in Fig. 3.4. The curve is divided into the three groups separated by the initial weights:  $W_0 \leq 0.045$ ,  $0.045 < W_0 < 0.055$ , and  $W_0 \geq 0.055$ . For  $W_0 \leq 0.045$ , the mean order parameter of the initial state has values  $\bar{R} \leq 0.11$ , indicating that the synchronization in the initial state is low or inexistent. It means that the mean order parameter related to this state is small as it smoothly enhances. In this cases, the initial synapses are not strong enough to synchronize the neurons in the network. When the plasticity is considered (red line),  $\bar{R}$  smoothly increases, even without initial synchronization. In particular, for  $W_0 = 0$ , when there is no interaction between the neurons before applying the plasticity rule, synapse potentiation is identified. At this point, the potentiation comes not from synchronization, but from a different phenomenon entirely, that is related to the natural neural frequencies. For this interval ( $W_0 \leq 0.045$ ), the potentiation is due to the coincidence of bursts of high-frequency neurons, which is called “Type I potentiation”.

For  $W_0 \geq 0.055$ , the mean order parameter of the initial state has values  $\bar{R} \geq 0.6$ , indicating the existence of burst synchronization. This occurs due to the fact that the initial state synapses are strong enough to synchronize the network right from the start. After applying the plasticity rule, an increase of  $\bar{R}$  for these  $W_0$  is observed. When the initial synchronization occurs, the mean synaptic weight will increase. It causes the neurons to burst at almost the same time and thus potentiate the synapses. This mechanism of potentiation via synchronization-caused burst coincidence is a “Type II potentiation”. As the synapses get stronger, the network becomes more synchronized, and as a consequence an increase on the order parameter is also observed. There is a positive feedback between synchronization and potentiation, and this feedback is the reason

that synaptic weights go to their maximum values. The synapses that connect synchronized neurons become stronger over time.

When the intermediate values of  $W_0$  are considered as  $0.045 < W_0 < 0.055$ , both Type I and II mechanisms appear. The mean order parameter of the initial state changes from 0.11 to 0.6, while it is in the interval  $[0.67, 0.77]$  for the final state. For the range related to the final state, a partial burst synchronization occurs between the neurons. There are some neurons that are synchronized to each other and their synapses are potentiated. There are also some high-frequency neurons that do not start synchronized to the others. The synapses between these neurons are also strengthened due to the coincidence of bursts. Then, there are two groups of synapses that are potentiated, where one is connected with synchronized neurons and the other that is connected with high-frequency neurons. However, the synapses connecting a high-frequency neuron to a synchronized neuron are not potentiated, but instead they are depressed. For this reason, in this regime, two separate clusters are identified, one that is composed of neurons that potentiate via Type I mechanism and the other via Type II mechanism.

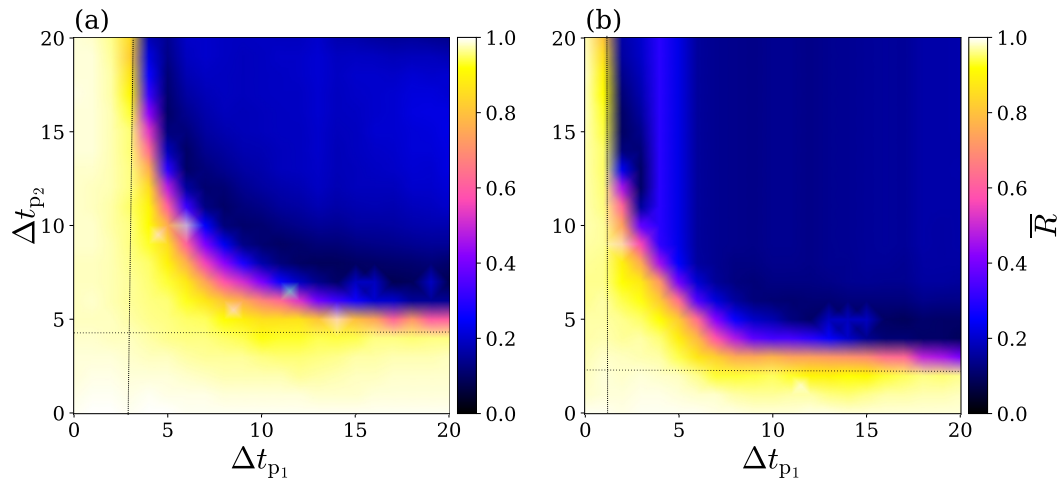
### 3.2.2 Effects of External Pulsed Perturbations in Bursting Synchronous Behavior

The effects of external perturbations in the random network formed according to the Erdős-Rényi model and influenced by the BTDP rule are investigated. Firstly, an external periodic pulsed current in the neural network with  $I_0 = 8 \mu\text{A}/\text{cm}^2$  and  $\Delta t_{p_1}$  and  $\Delta t_{p_2}$  varying in the interval  $[0, 20]$  ms, as exhibited in Fig. 3.5, is applied. Figures 3.5(a) and 3.5(b) exhibit  $\bar{R}$  in color scale for the two different amplitudes,  $\tau = 0.3$  and  $\tau = 0.5 \mu\text{A}/\text{cm}^2$ , respectively. In Fig. 3.5(a), the neurons are synchronized with each other for small values of  $\Delta t_{p_1}$  and  $\Delta t_{p_2}$ , while the desynchronization among them occurs when  $\Delta t_{p_1} \geq 3.0$  ms and  $\Delta t_{p_2} \geq 4.5$  ms. On the other hand, it is observed that desynchronization begins from  $\Delta t_{p_1} \geq 1.5$  ms and  $\Delta t_{p_2} \geq 2.5$  ms in Fig. 3.5(b). As a consequence, various values considered for the time duration can decrease the mean order parameter and suppress synchronous behavior in the random network influenced by the BTDP rule.

Moreover, the dynamical behavior of the neurons under an external random pulsed current is analyzed. Figure 3.6 shows the time-averaged order parameter in color scale for  $\Delta t_i$  randomly distributed in the interval  $[0, 20]$  ms with  $I_0$  and  $\tau$  varying in the range  $[8, 15]$  and  $[0, 2]$ , respectively. Therefore, there are no significant alterations in the synchronous behavior by varying  $I_0$  in the range  $[8, 15]$ . However, the values of  $\tau$  approximately larger than 0.27 are able to suppress neural synchronization.

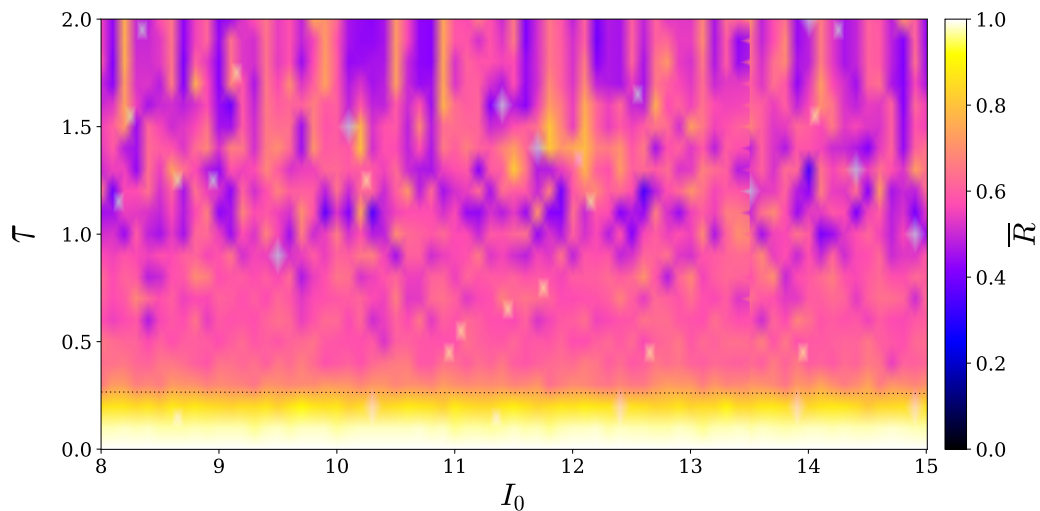
In summary, our numerical simulations show that both mean synaptic weight and time-averaged order parameter as a function of the initial weights enhance when the high-frequency bursts occur or the synapses become strong enough between synchronized neurons. Furthermore, the external pulsed currents play an important role in changing burst synchronization.

Figure 3.5:  $\Delta t_{p_2} \times \Delta t_{p_1}$  for (a)  $\tau = 0.3 \mu\text{A}/\text{cm}^2$  and (b)  $\tau = 0.5 \mu\text{A}/\text{cm}^2$  with  $I_0 = 8 \mu\text{A}/\text{cm}^2$  to represent  $\bar{R}$  in color scale for the plastic network under a periodic external current. Depending on the time duration, synchronous behavior can be suppressed in the random network.



Source: The author.

Figure 3.6: Mean order parameter (color scale) in the parameter space  $\tau \times I_0$  of coupled neurons under a random pulsed perturbation with  $\Delta t_r$  randomly distributed in the interval  $[0, 20]$  ms. It is not observed a significant alteration in the synchronization by varying  $I_0$ .



Source: The author.

## 4 RESEARCH AREA 2

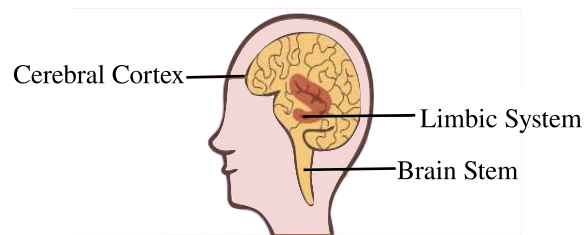
The human brain is a complex organ responsible for cognitive processes and physiological functions. It contains about 100 billion neurons that are coupled by means of electrical and chemical synapses. The electrical synapse is a bidirectional link between two neighboring neurons. In the chemical synapse, neural impulses are transferred in one way by means of neurotransmitters. The neurons connected to each other form a large layered network in which the different cortical and non-cortical layers in one hemisphere have connections with other ones in another hemisphere. In this chapter, the main purpose is the study of burst synchronization and desynchronization in a neural network model composed of 83 subnetworks available in both hemispheres and brain stem of a human brain. Likewise, a neural network based on the structural connectivity matrix of a human brain is built. The network is composed of cortical regions in which each region is described by subnetworks with small-world properties. Depending on the parameters, it is possible to observe synchronous and desynchronous behaviors. Also, the effects of periodic and random pulsed currents in the neural activities are analyzed. It is shown that pulsed currents play an important role in the emergence and suppression of neural synchronization.

### 4.1 NETWORK OF SMALL-WORLD NETWORKS MODEL

The network selected for the study consists of 83 nodes corresponding to different cortical and non-cortical regions, and brain stem as illustrated in Fig. 4.1, where each node has 120 neurons described by the Rulkov model. A structural connectivity matrix according to the brain of a healthy individual from <https://braingraph.org> (113–115) is used to build a neural network model containing the organization of connections between the different brain regions. The connection matrix, presenting a weighted matrix, whose values represent the number of fibers. Figure 4.2 illustrates how nodes in the brain connect to other nodes, where the color code represents the number of fibers. The symmetry adjacency matrix demonstrates the connections between the 83 regions located at the cortex surface and limbic system for both right and left hemispheres, and also brain stem. The regions from 1 to 41 are related to the right hemisphere, from 42 to 82 are located at the left hemisphere, and the region with the number 83 is considered for the brain stem. By considering the matrix, a new matrix with only five numbers in different colors is built, as shown in Fig. 4.3. The number 0 (white) shows that there is no connection between the two cortical regions. The numbers 1 (red), 2 (green), 3 (blue) and 4 (black) represent the weak, intermediate, normal and strong connections between the cortical areas, respectively. These numbers are based on the work published by Scannell and Young (49). They reported the connectional organization of neural systems in the cat cerebral cortex. The regions with white, red, green, blue, and black colors have no connections, 50, 100, 150, and 200 connections with

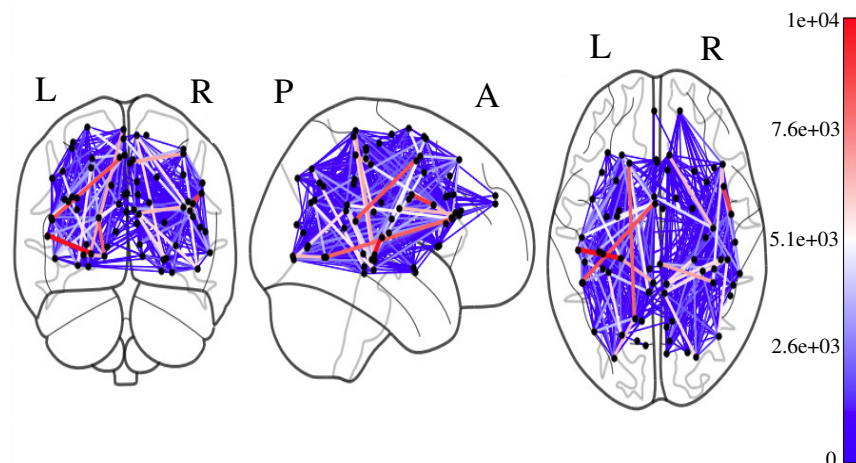


Figure 4.1: Illustration of cerebral cortex located at the cortical regions, limbic system located at the non-cortical regions, and brain stem in the brain.



Source: Adapted from (112).

Figure 4.2: Connectome in the direction of the cuts:  $y$  (coronal),  $x$  (sagittal), and  $z$  (axial), respectively, for a healthy subject. The color bar indicates the amount of weights described as the number of fibers. Only 15% of the connections are considered, due to the fact that the graphs are very dense.  $L$  and  $R$  indicate the left and right hemispheres, respectively.  $P$  and  $A$  depict the posterior and anterior of the brain, respectively.

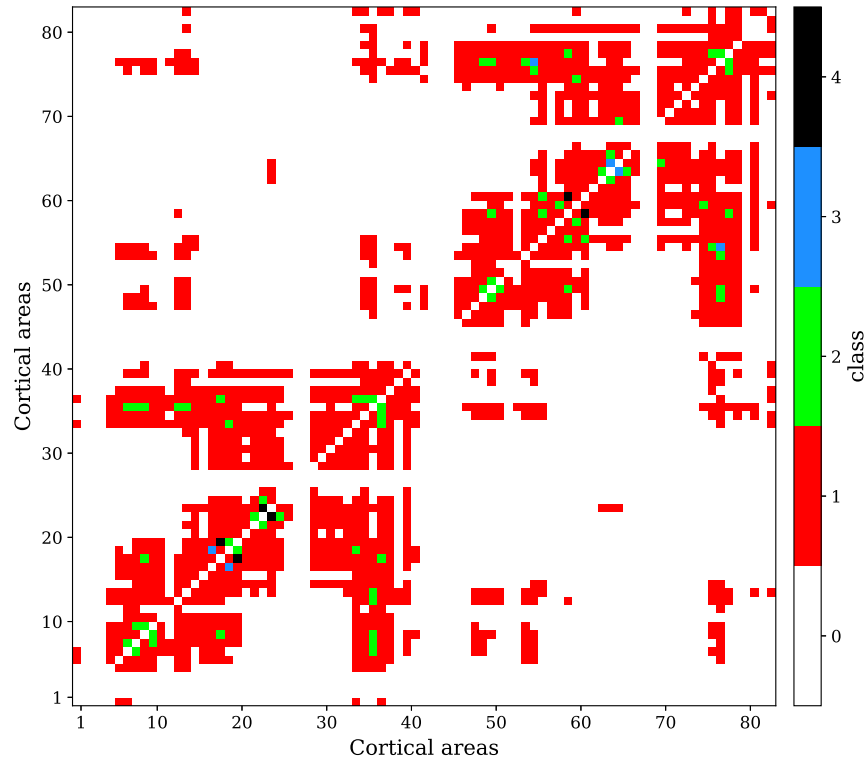


Source: The author.

other regions, respectively. The connections are randomly selected. The numbers 1, 2, 3, and 4 have been classified according to the number of fibers in the interval  $[1, 3000]$ ,  $[3001, 6000]$ ,  $[6001, 9000]$  and more than 9000, respectively, from the structural connectivity matrix of the brain.

Each cortical region is represented by a subnetwork with small-world properties. The small-world network has a combination of short path length comparable to a random network and high clustering as a regular network (33). According to these features, small-world networks have been applied in various researches related to the connectivity of the nervous system (37, 47). In this work, the small-world network introduced by Newman and Watts is used to build subnetworks containing 120 neurons connected to their 4 nearest neighbors with the probability distribution  $p = 0.2$ . In the Newman-Watts model, there is no probability of a part of the network becomes disconnected from the rest. In the small-world subnetworks, the electrical coupling is

Figure 4.3: Structural connection matrix related to the 83 areas in the brain of a healthy human. The areas start from 1 to 41 for the right hemisphere, from 42 to 82 for the left hemisphere, and with the number 83 for the brainstem.



Source: The author.

just between the nearest neighbors (local), while the chemical connections only provide the shortcuts (non-local) considered by the probability distribution. The links between the small-world subnetworks follow the cortical connectome of the brain, as shown in Fig. 4.3.

With regard to the connections among the neurons, the couplings can be electrical or chemical. The chemical coupling can be excitatory or inhibitory. Within each small-world subnetwork, there are local and non-local connectivities that describe the electrical and chemical synapses, respectively. The connections between each subnetwork are non-local links based on the chemical synapses.

The mathematical model is given by

$$x_{t+1}^{(i,p)} = \frac{\alpha^{(i,p)}}{1 + (x_t^{(i,p)})^2} + y_t^{(i,p)} + \frac{e}{2}(x_t^{(i-1,p)} + x_t^{(i+1,p)} - 2x_t^{(i,p)}) - c \sum_{j=1}^N \sum_{f=1}^P [A_{(j,f),(i,p)} H(x_t^{(j,f)} - \varphi)(x_t^{(i,p)} - R_s)] + \Lambda_t^{(i,p)}, \quad (4.1)$$

$$y_{t+1}^{(i,p)} = y_t^{(i,p)} - \delta(x_t^{(i,p)} - \beta), \quad (4.2)$$

where the initial conditions for the variables  $x_i$  and  $y_i$  are randomly selected from  $[-2, 2]$  and  $[-4, 0]$ , respectively. The pair  $(i, p)$  shows the neuron  $i$  ( $i = 1, 2, \dots, N$ ) in the brain area  $p$  ( $p = 1, 2, \dots, P$ ), where  $N = 120$  is the number of neurons in each subnetwork and  $P = 83$  is the number of brain areas. The connectivity matrix is given by  $A_{(j,f),(i,p)}$ , corresponding to the chemical coupling. When the neuron  $(j, f)$  connects with the neuron  $(i, p)$ , the element of the matrix is equal to 1, otherwise is equal to zero. The  $\alpha^{(i,p)}$  value is the non-linearity parameter of the Rulkov model randomly selected from  $[4.1, 4.4]$ . The values of  $\alpha^{(i,p)}$  are distributed using a random uniform generator. It is considered  $\delta = 0.001$  and  $\beta = -1.25$ . Furthermore,  $e$  and  $c$  are associated with the electrical and chemical coupling strengths, respectively.  $H(x)$  is the Heaviside step function with the presynaptic threshold equal to  $\varphi = -1.0$  for the chemical synapse. When the presynaptic neuron voltage is greater than  $\varphi$ , the post-synaptic neuron receives an input. The constant  $R_s$  is described by the nature of the post-synaptic ion channels and determines the reversal potential related to the synapse. In 1984, Feldman (116) reported that approximately 70 – 80% of the neural population of the cortex is excitatory. If  $R_s = 1$  or  $-2$ , the synapse is excitatory or inhibitory, respectively. These values of  $R_s$  are randomly distributed in whole network that in such way 75% and 25% of connections, respectively, are excitatory and inhibitory (117). A single neuron does not make both excitatory and inhibitory connections with other neurons. Finally,  $\Lambda_t^{(i,p)}$  is an external pulsed perturbation that activates the spikes in the neurons. The Rulkov neurons are stimulated over time  $t$  by periodic and random pulses considered as an external pulsed current as described by Eq. 2.24.

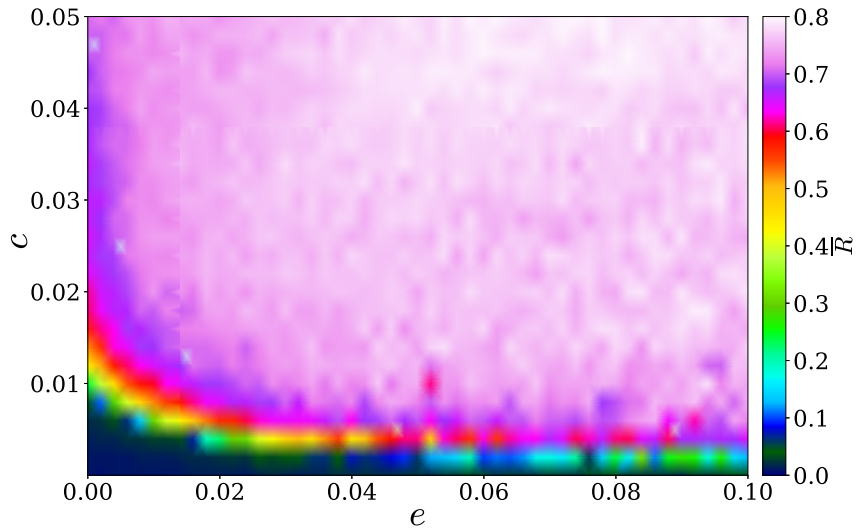
## 4.2 RESULTS

### 4.2.1 Burst Synchronization without Pulses

In the central nervous system, bursts and oscillatory patterns of neural activities can be observed from slow to fast oscillations (118). In this work, it is focused on the burst phase synchronization, which is a type of neural synchronization (119). It is possible to identify phase synchronization related to bursts of neural ensemble by means of the Kuramoto order parameter (105), as described by Eqs. 2.22 and 2.23.

With regard to the neural network for an individual, the values of the time-averaged order parameter (color scale) as a function of the electrical and chemical coupling strengths are displayed in Fig. 4.4. This figure shows the coupling strength ranges in which the network exhibits synchronous behavior. The neural network does not exhibit a completely phase synchronized state ( $\overline{R} = 1$ ), due to the fact that the neurons are not identical. According to the network synchronization diagnostic of the dynamics, the regions for  $\overline{R} < 0.8$  show desynchronous behavior, while synchronous behavior occurs for  $\overline{R} \geq 0.8$ . The increase of the chemical coupling  $c$  leads the network to the neural synchronization.

Figure 4.4: Time-averaged order parameter (color bar) as a function of  $c$  (chemical synapses) in the interval  $[0, 0.05]$  and  $e$  (electrical synapses) in the range  $[0, 0.1]$  of the human's brain areas during  $10^6$  iterations.



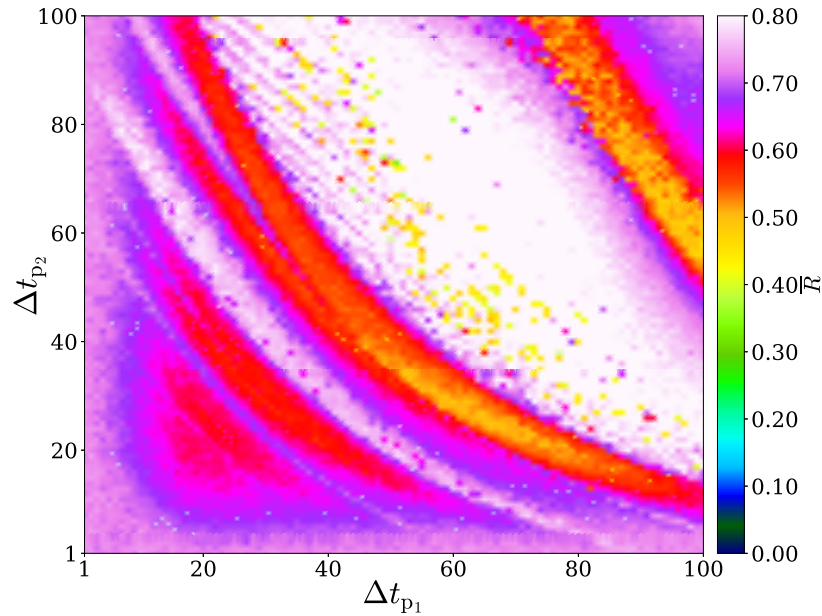
Source: The author.

#### 4.2.2 Applying External Pulsed Perturbations in Bursting Synchronization

It has been reported that external pulsed currents can cause changes in neural synchronous behavior, as well as alterations in neuron spiking activities (73, 120). With this in mind, the effect of external pulsed perturbations, as described in Eq. (2.24), in the brain network model considering  $e = 0.1$  and  $c = 0.05$ , as shown in Fig. 4.5, is investigated. Figure 4.5 displays the effect of periodic pulses with  $I_0 = 8$ ,  $\tau = 0.1$ , and  $\Delta t_{p_1}$  and  $\Delta t_{p_2} \in [1, 100]$  ms, which represent the on and off intervals in the periodic pulse profile, respectively. The periodic perturbation induces a change in the synchronous behavior and reduces the value of the time-averaged order parameter in some areas. The results show that alterations related to  $\Delta t_{p_1}$  and  $\Delta t_{p_2}$  play an important role in the synchronous patterns. In other words, depending on the combination of  $\Delta t_{p_1}$  and  $\Delta t_{p_2}$ , synchronization and desynchronization can emerge in all the network.

Considering the impact of the periodic pulses in the whole brain, it is investigated how this external perturbation influences the synchronous behavior in the regions from 1 to 34, from 35 to 41, from 42 to 75, from 76 to 82, and 83, as exhibited in Fig. 4.6 from the panels (a) to (d), and Fig. 4.7, respectively. For the cortical areas in the right hemisphere, Fig. 4.6(a) displays that, for instance, the burst desynchronization with  $\bar{R}$  about 0.4 and 0.6 starts from the time intervals greater than  $\Delta k_1 \approx 20$  ms and  $\Delta k_2 \approx 10$  ms, and continues until the center of the figure and around it. The synchronous behavior for the non-cortical areas in the right hemisphere is not suppressed when the on-off intervals change, except on some combinations of them with the time-averaged order parameter about 0.6 dispersed in Fig. 4.6(b). Regarding the cortical and non-cortical areas in the left hemisphere, the bursting synchronization and desynchronization

Figure 4.5: Averaged order parameter of the human's brain network under a periodic pulse with  $I_0 = 8 \mu\text{A}/\text{cm}^2$  and  $\tau = 0.1 \mu\text{A}/\text{cm}^2$  in the parameter space  $\Delta t_{p_2} \times \Delta t_{p_1}$  varying in the interval  $[1, 100]$  ms for the synchronized point  $e = 0.1$  and  $c = 0.05$ .



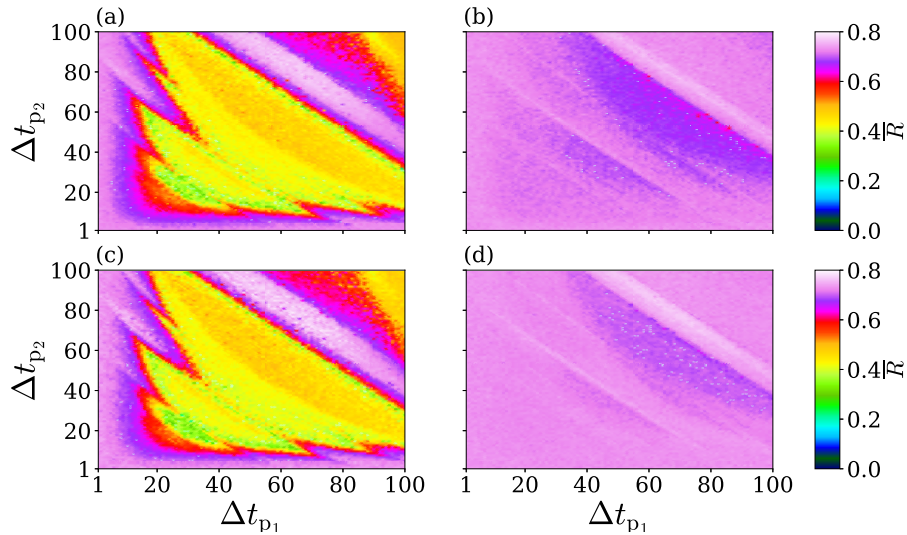
Source: The author.

(Figs. 4.6(c) and 4.6(d)) are very similar to the behaviors observed in Figs. 4.6(a) and 4.6(b), except some points indicating more synchronous behavior with the light purple color scale dispersed in the middle of the figure. In Fig. 4.7, it is observed neural synchronous behavior with  $\bar{R}$  close to 0.8.

The effect of random perturbations, as another type of external pulsed current, is investigated. Random pulses with  $I_0 = 8$ ,  $\tau \in [0, 4]$  and  $\Delta t_r$  randomly distributed in the interval  $[20, 100]$  are considered. To investigate the neural synchronous behavior in the whole brain network under a random current, the time-averaged order parameter  $\bar{R}$ , as displayed in Fig. 4.8, is calculated. Increasing  $\tau$  approximately from 0.1 to 2, the bursting synchronization is suppressed for almost all the values related to  $\Delta t_r$ . The burst synchronous behavior does not change for about  $\tau > 2$  and alterations in the on-off time intervals have no substantial effect on the synchronization. For  $\tau < 2$ , the parameter regions in which synchronization appears are observed.

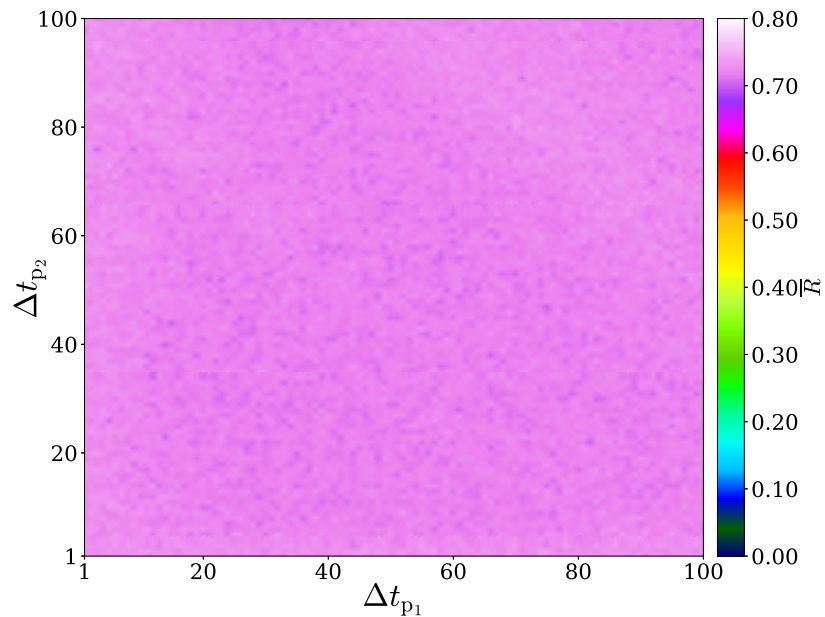
In order to study the bursting synchronous behavior, an external current with random pulses in the 5 regions is applied. In Fig. 4.9, desynchronization ( $\bar{R}$  equal or close to 0.4 or 0.6) in the four regions exhibited in the panels (a), (b), (c), and (d) is appeared. The desynchronization occurs for all the amplitudes, except for  $\tau = 0.1$ . Figure 4.9(d) shows the time-averaged order parameter greater than the panels (a), (b), and (c). Furthermore, the random perturbation applied in the region 83 (brain stem) of the brain changes the synchronization in the whole region with  $\bar{R}$  approximately equal to 0.7, as shown in Fig. 4.10. The bursting synchronization does not

Figure 4.6: Time-averaged order parameter of the whole brain network grouped into regions from (a) 1 to 34, (b) 35 to 41, (c) 42 to 75, and (d) 76 to 82. A periodic pulsed current with  $I_0 = 8 \mu\text{A}/\text{cm}^2$  and  $\tau = 0.1 \mu\text{A}/\text{cm}^2$  in the parameter space  $\Delta t_{p_2} \times \Delta t_{p_1}$  varying in the interval  $[1, 100]$  ms for  $e = 0.1$  and  $c = 0.05$ , which indicates the bursting synchronization, is considered.



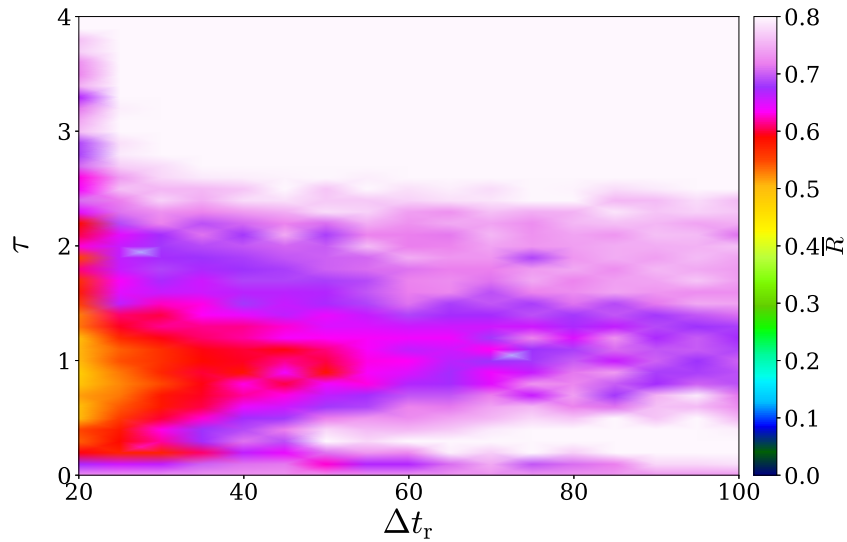
Source: The author.

Figure 4.7: Time-averaged order parameter of the region 83 by considering a periodic pulsed perturbation with  $I_0 = 8 \mu\text{A}/\text{cm}^2$ , and  $\tau = 0.1 \mu\text{A}/\text{cm}^2$  in the parameter space  $\Delta t_{p_2} \times \Delta t_{p_1}$  varying in the interval  $[1, 100]$  ms for  $e = 0.1$  and  $c = 0.05$  indicating the burst synchronous behavior.



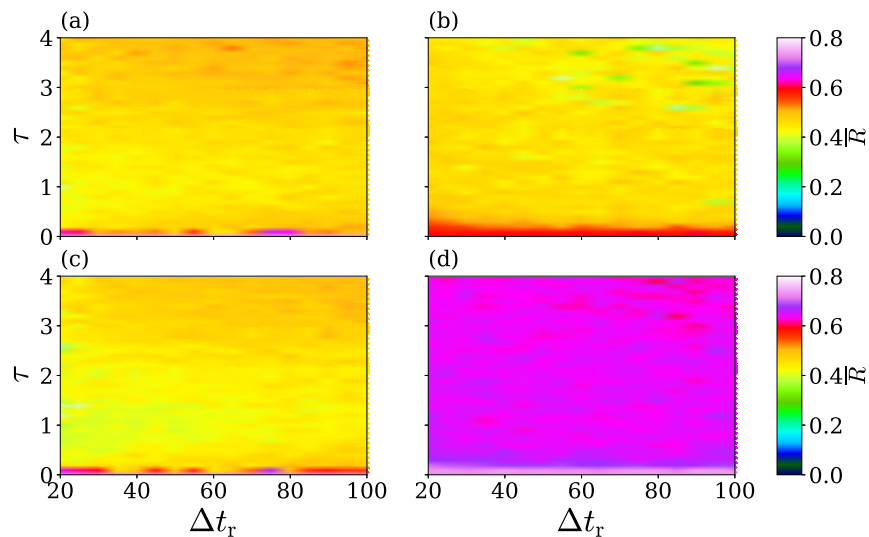
Source: The author.

Figure 4.8: Averaged order parameter of the whole brain network under a random pulsed current as a function of  $\tau$  and  $\Delta t_r$  changing in the interval  $[0, 4] \mu\text{A}/\text{cm}^2$  and  $[20, 100]$  ms, respectively, for  $I_0 = 8 \mu\text{A}/\text{cm}^2$ ,  $e = 0.1$ , and  $c = 0.05$ .



Source: The author.

Figure 4.9: Time-averaged order parameter of the four cortical regions of the brain network from (a) 1 to 34, (b) 35 to 41, (c) 42 to 75, and (d) 76 to 82, by considering a random pulsed perturbation with  $\tau$  and  $\Delta t_r$  in the interval  $[0, 4] \mu\text{A}/\text{cm}^2$  and  $[20, 100]$  ms, respectively, for  $I_0 = 8 \mu\text{A}/\text{cm}^2$ ,  $e = 0.1$ , and  $c = 0.05$ .

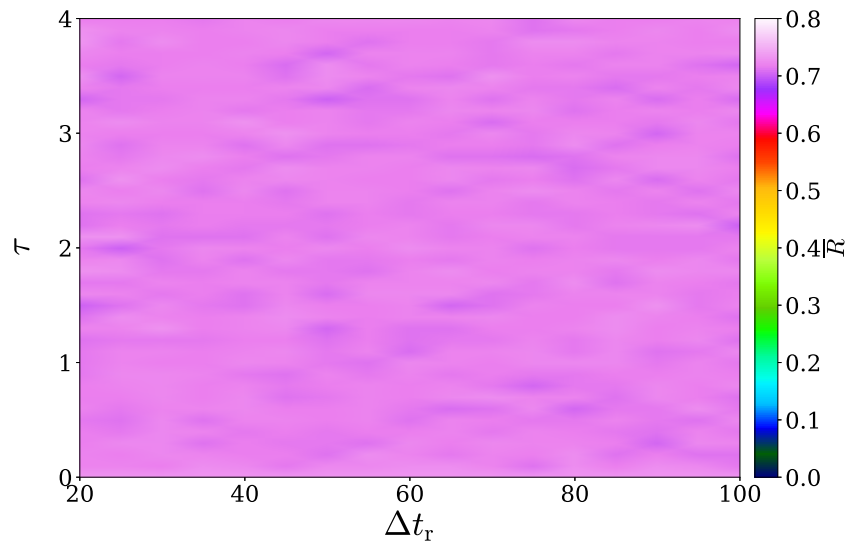


Source: The author.

depend on  $\tau$  and  $\Delta t_r$ .

In summary, the numerical simulations show that the external pulsed perturbations generated by electrodes in the brain, also known as deep brain stimulation, not only can have a relevant

Figure 4.10: Time-averaged order parameter of the region 83 of the brain network under a random pulsed current for  $\tau$  and  $\Delta t_r$  selected from the interval  $[0, 4] \mu\text{A}/\text{cm}^2$  and  $[20, 100]$  ms, respectively. It is considered  $I_0 = 8 \mu\text{A}/\text{cm}^2$ ,  $e = 0.1$ , and  $c = 0.05$ .



Source: The author.

effect on the dynamics of neurons in the network based on a human's brain areas, but also can create changes in the emergence of spike activities and bursting synchronization.



## 5 FINAL REMARKS

Throughout this thesis, the main goals are to demonstrate the emergence of bursting synchronization and desynchronization in two different neural networks, and also to show the effect of external periodic and random pulsed currents on neural activities related to pathological synchronous behavior. In this sense, two different network topologies, one influenced by burst-timing-dependent plasticity and another one built according to the structural connectivity matrix of a healthy human brain, have been considered.

In Chapter 3 as Research Area 1, a random neural network based on the Erdős-Rényi model was built. The neurons were connected by means of a pre-determined probability distribution. The chemical excitatory synapses among the neurons were quantified with initial weight values and updated by the time difference between the burst-start points related to presynaptic and postsynaptic neurons, namely burst-timing-dependent plasticity (BTDP). The relation between the potentiation and burst synchronization for different initial weights in the network with BTDP was investigated. Two types of potentiations in the simulations were identified. In the Type I potentiation, there was no synchronous behavior, while the Type II potentiation was induced by the synchronization. Previous studies have reported the emergence of bursting synchronization in networks with BTDP (66, 68). Furthermore, periodic and random pulses as external perturbations were considered to study how they influence the bursting synchronous behavior. In the numerical simulations, it was shown that both mean synaptic weight and time-averaged order parameter as a function of the initial weights enhance when the high-frequency bursts occur or the synapses become strong enough between synchronized neurons. Furthermore, the external pulsed currents played an important role in changing burst synchronization. It was demonstrated that that pulsed currents can be an effective method to suppress neural synchronization in a plastic network. There are experimental evidences that pulsed currents generated by electrodes in the brain, known as deep brain stimulation, can be used to treat some neurological conditions (108).

In Chapter 4 as Research Area 2, a neural network model based on the healthy human brain cortical and non-cortical areas, and brain stem was designed. The network was composed of 83 small-world subnetworks of coupled Rulkov neurons for each brain area. In the network, each neuron can have local and non-local connections with other neurons by means of electrical and chemical synapses, respectively. Without external pulsed currents, the neurons can exhibit synchronization between themselves due to the synaptic interaction. With regard to the external perturbation with periodic pulses, the neural activities depend on the pulse duration. For the random pulsed currents, a reduced time-averaged order parameter was observed when the pulse amplitude changes. The results were robust due to the fact that it was considered not only different nonlinearity parameter values in the range in which the neurons exhibit chaotic bursts, but also the initial conditions were randomly distributed. The results had some similarities with the outcomes obtained by Lameu et al. (30) for a clustered scale-free neural networks based

on the cat cortex structure. The neurons in the whole networks exhibited synchronous patterns when the coupling strength is increased. Depending on the external perturbation, it is observed regions with synchronous behavior while others remained desynchronized. An external pulsed current which permits a better control on the synchronization was considered, due to the fact that the pulse amplitude and time interval can be chosen freely.

Overall, It was demonstrated that the burst-timing-dependent plasticity as a type of neuroplasticity and the synaptic interaction between presynaptic and postsynaptic neurons, and also between subnetworks can exhibit the formation and destruction of bursting neural synchronization in the network models, as well as that the external pulsed currents can be an effective method to suppress bursting neural synchronization in the neural networks with variant topologies.

The results of this thesis offer various directions for further research. It will be worthwhile to investigate the effect of external pulsed currents on a network built according to the structural connectivity matrix of two human brains diagnosed with Alzheimer's disease and brain tumor. After that, it can be a good work to compare the brain regions indicating synchronization and desynchronization with those identified by a healthy subject. Furthermore, the emergence of bursting synchronization and desynchronization in a network influenced by neurogenesis and the effect of external pulsed currents on the network can be valuable when the results are compared with those results obtained from the plastic network.

## REFERENCES

- 1 EROGLU, D.; LAMB, J. S. W.; PEREIRA, T. Synchronisation of chaos and its applications. **Contemporary Physics**, vol. 58, no. 3, p. 207-243, 2017.
- 2 BENNETT, M.; SCHATZ, M. F.; ROCKWOOD, H.; WIESENFELD, K. Huygens's clocks. **Proceedings: Mathematical, Physical and Engineering Sciences**, vol. 458, no. 2019, p. 563-579, 2002.
- 3 PECORA, L. M.; CARROLL, T. L. Synchronization in chaotic systems. **Physical Review Letters**, vol. 64, no. 8, p. 821, 1990.
- 4 GOLDBETER, A. **Biochemical oscillations and cellular rhythms: the molecular bases of periodic and chaotic behaviour**. Cambridge University Press, 1997.
- 5 PIKOVSKY, A.; ROSENBLUM, M.; KURTHS, J. **Synchronization: a universal concept in nonlinear sciences**. Cambridge University Press, 2003.
- 6 BUCK, J.; BUCK, E. Synchronous fireflies. **Scientific American**, vol. 234, no. 5, p. 74-85, 1976.
- 7 WALKER, T. J. Acoustic synchrony: two mechanisms in the snowy tree cricket. **Science**, vol. 166, no. 3907, p. 891-894, 1969.
- 8 FELL, J.; AXMACHER, N. The role of phase synchronization in memory processes. **Nature Reviews Neuroscience**, vol. 12, no. 2, p. 105-118, 2011.
- 9 GLASS, L. Synchronization and rhythmic processes in physiology. **Nature**, vol. 410, no. 6825, p. 277-284, 2001.
- 10 WANG, X. J. Neurophysiological and computational principles of cortical rhythms in cognition. **Physiological Reviews**, vol. 90, no. 3, p. 1195-1268, 2010.
- 11 HUTCHEON, B.; YAROM, Y. Resonance oscillation and the intrinsic frequency preferences of neurons. **Trends in Neuroscience**, vol. 23, no. 5, p. 216-222, 2000.
- 12 MELLONI, L.; MOLINA, C.; PENA, M.; TORRES, D.; SINGER, W.; RODRIGUEZ, E. Synchronization of neural activity across cortical areas correlates with conscious perception. **Journal of Neuroscience**, vol. 27, no. 11, p. 2858-2865, 2007.
- 13 HIPPEL, J. F.; ENGEL, A. K.; SIEGEL, M. Oscillatory synchronization in large-scale cortical networks predicts perception. **Neurons**, vol. 69, no. 2, p. 387-296, 2011.

- 14 GRAMMONT, F.; RIEHLE, A. Spike synchronization and firing rate in a population of motor cortical neurons in relation to movement direction and reaction time. **Biological Cybernetics**, vol. 88, no. 3, p. 360-373, 2003.
- 15 LESTIENNE, R. Spike timing, synchronization and information processing on the sensory side of the central nervous system. **Prog. Neurobiol.**, vol. 65, p. 545-91, 2001.
- 16 KANDEL, E. R.; SCHWARTZ, J. H.; JESSELL, T. M.; SIEGELBAUM, S. A.; HUDSPETH, A. J. **Principles of Neural Science**. Fifth. McGraw-hill New York, 2013.
- 17 MORMANN, F.; LEHNERTZ, K.; DAVID, P.; ELGER, C. E. Mean phase coherence as a measure for phase synchronization and its application to the EEG of epilepsy patients. **Physica D: Nonlinear Phenomena**, vol. 144, no. 3, p. 358-369, 2000.
- 18 HAMMOND, C; BERGMAN, H.; BROWN, P. Pathological synchronization in Parkinson's disease: networks, models and treatments. **Trends in Neurosciences**, vol. 30, no. 7, p. 357-364, 2007.
- 19 POPOVYCH, O. V.; TASS, P. A. Control of abnormal synchronization in neurological disorders. **Frontiers in Neurology**, vol. 5, p. 268, 2014.
- 20 DINSTEIN, I.; PIERCE, K.; EYLER, L.; SOLSO, S.; MALACH, R.; BEHRMANN, M.; COURCHESNE, E. Disrupted neural synchronization in toddlers with autism. **Neuron**, vol. 70, no. 6, p. 1218-1225, 2011.
- 21 GREICIUS, M. D.; SRIVASTAVA, G.; REISS, A. L.; MENON, vol. Default-mode network activity distinguishes Alzheimer's disease from healthy aging: evidence from functional MRI. **Proceedings of the National Academy of Sciences**, vol. 101, no. 13, p. 4637-4642, 2004.
- 22 SALADIN, K. S. **Human anatomy (3rd ed.)**. McGraw-Hill, p. 416, 2011.
- 23 TORTORA, G. J.; DERRICKSON, B. **Principles of Anatomy and Physiology**. John Wiley press, 2016.
- 24 KOCH, C.; SEGEV, I. The role of single neurons in information processing. **Nat. Neurosci.**, vol. 3, p. 1171-1177, 2000.
- 25 KANDEL, E. R.; SCHWARTZ, J. H.; JESSELL, T. M. **Ch. 9: Propagated signaling: the action potential**. Principles of Neural Science, 2000.
- 26 SMITH, M.; PEREDA, A. E. Chemical synaptic activity modulates nearby electrical synapses. **PNAS**, vol. 100, p. 4849-4854, 2003.

- 27 KOPELL, N.; ERMENTROUT, B. Chemical and electrical synapses perform complementary roles in the synchronization of interneuronal networks. **PNAS**, vol. 101, p. 15482-15487, 2004.
- 28 RULKOV, N. F. Regularization of Synchronized Chaotic Bursts. **Physical Review Letters**, vol. 86, no. 1, p. 183-186, 2001.
- 29 BATISTA, C. A. S.; LAMEU, E. L.; BATISTA, A. M.; LOPES, S. R.; PEREIRA, T.; ZAMORA-LOPES, G.; KURTHS, J.; VIANA, R. L. Phase synchronization of bursting neurons in clustered small-world networks. **Phys. Revol. E**, vol. 86, p. 016211, 2012.
- 30 LAMEU, E. L.; BATISTA, C. A. S.; BATISTA, A. M.; IAROSZ, K. C.; VIANA, R. L.; Lopes, S. R.; KURTHS, J. Suppression of bursting synchronization in clustered scale-free (rich-club) neuronal networks. **Chaos**, vol. 22, p. 043149, 2012.
- 31 BATISTA, C. A. S.; Lopes, S. R.; VIANA, R. L.; BATISTA, A. M. Delayed feedback control of bursting synchronization in a scale-free network. **Neural Network**, vol. 23, p. 114-24, 2010.
- 32 ERDÖS, P.; RÉNYI, A. On random graphs. **Publ. Math. Debrecen**, vol. 6, p. 290, 1959.
- 33 WATTS, D. J.; STROGATZ, S. H. Collective dynamics of small-world networks. **Nature**, vol. 393, p. 440-442, 1998.
- 34 Newman, M. E. J.; Watts, D. J. Renormalization group analysis of the small-world network model. **Phys. Lett. A**, vol. 263, p. 341-346, 1999.
- 35 VIANA, R. L.; BORGES, F. S.; IAROSZ, K. C.; BATISTA, A. M.; LOPES, S. R.; CALDAS, I. L. Dynamic range in a neuron network with electrical and chemical synapses. **Commun. Nonlinear Sci. Numer. Simul.**, vol. 19, p. 164-172, 2014.
- 36 REIS, A. S.; BRUGNAGO, E. L.; VIANA, R. L.; BATISTA, A. M.; IAROSZ, K. C.; CALDAS, I. L. Effects of feedback control in small-world neuronal networks interconnected according to a human connectivity map. **Neurocomputing**, vol. 518, p. 321-331, 2023.
- 37 BASSETT, D. S.; BULLMORE, E. Small-world brain networks. **Neuroscientist**, vol. 12, p. 512-523, 2006.
- 38 WATTS, D. J. Networks, dynamics, and the Small-World phenomenon. **Am. J. Sociol.**, vol. 105, p. 493-527, 1999.
- 39 VARSHNEY, L. R.; CHEN, B. L.; PANIAGUA, E.; HALL, D. H.; CHKLKOVSHII, D. B. Structural properties of the *Caenorhabditis elegans* neuronal network. **PLoS Comput. Biol.**, vol. 7, p. e1001066, 2011.

- 40 ROCKEL, A. J.; HIORNS, R. W.; POWELL, T. P. S. The basic uniformity in structure of the neocortex. **Brain**, vol. 103, p. 221-4, 1980.
- 41 ROLAND, P. E.; ZILLES, K. Structural divisions and functional fields in the human cerebral cortex. **Brain Res. Rev.**, vol. 26, p. 87-105, 1998.
- 42 WATTS, D. J. **Small worlds**. Princeton: Princeton University Press, 2011.
- 43 ZHOU, C.; ZEMANOVA, L.; ZAMORA-LOPEZ, G.; HILGETAG, C. C.; KURTHS, J. Structure-function relationship in complex brain networks expressed by hierarchical synchronization. **New J. Phys.**, vol. 9, p. 178, 2007.
- 44 XU, J.; ZHANG, S.; CALHOUN, D.; MONTEROSSO, J.; LI, C. S. R.; WORHUNSKY, D.; STEVENS, M.; PEARLSON, G. D.; POTENZA, M. Task-related concurrent but opposite modulations of overlapping functional networks as revealed by spatial ICA. **NeuroImage**, vol. 79, p. 62-71, 2013.
- 45 DECO, G.; BUEHLMAN, A.; MASQUELIER, T.; HUGUES, E. The role of rhythmic neural synchronisation in rest and task conditions. **Front. Hum. Neurosci.**, vol. 5, p. 4, 2011.
- 46 JIANG, J.; DAI, B.; PENG, D.; ZHU, C.; LIU, L.; LU, C. Neural synchronisation during face-to-face communication. **J. Neurosci.**, vol. 32, p. 16064-16069, 2012.
- 47 ACHARD, J.; SALVADOR, R.; Whitcher, B.; SUCKLING, J.; BULLMORE, E. A resilient, low-frequency, small-world human brain functional network with highly connected association cortical hubs. **J. Neurosci.**, vol. 26, p. 63-72, 2006.
- 48 SCANNELL, J. W.; BLAKEMORE, C.; YOUNG, M. Analysis of connectivity in the cat cerebral cortex. **J. Neurosci.**, vol. 15, p. 1463-83, 1995.
- 49 SCANNELL, J. W.; YOUNG, M. The connectional organization of neural systems in the cat cerebral cortex. **Current Biology**, vol. 3, p. 191-200, 1993.
- 50 HILGETAG, C. C.; BURNS, G. A. C.; ONEILL, M. A.; SCANNELL, J. W.; YOUNG, M. Anatomical connectivity defines the organization of clusters of cortical areas in the macaque monkey and the cat. **Philos. Trans. R. Soc. Lond. B. Biol. Sci.**, vol. 355, p. 91-110, 2000.
- 51 HE, Y.; CHEN, Z. J.; EVANS, A. C. Small-world anatomical networks in the human brain revealed by cortical thickness from MRI. **Cereb Cortex**, vol. 17, p. 2407-19, 2007.
- 52 SUN, X.; LEI, J.; PERC, M.; KURTHS, J.; CHEN, G. Burst synchronization transitions in a neuronal network of subnetworks. **Chaos**, vol. 21, p. 016110, 2011.

- 53 LAMEU, E. L.; BORGES, F. S.; BORGES, R. R.; BATISTA, A. M.; BAPTISTA, M. S.; VIANA, R. L. Network and external perturbation induce burst synchronisation in cat cerebral cortex. **Communo. Nonlinear Sci. Numer. Simul.**, vol. 34, p. 45-54, 2016.
- 54 MATEOS-APARACIO, P.; RODRIGUEZ-MORENO, A. The impact of studying brain plasticity. **Front. Cell. Neurosci.**, vol. 13, p. 66, 2019.
- 55 JAMES, W. **The Principles of Psychology**. Harvard University Press, 1890.
- 56 DEFELIPE, J. Brain plasticity and mental processes: cajal againo. **Nat. Rev. Neurosci.**, vol. 7, p. 811-817, 2006.
- 57 LASHLEY, K. S. The behavioristic interpretation of consciousness I. **Psychol. Rev.**, vol. 30, p. 237-272, 1923.
- 58 HEBB, D. O. **The Organization of Behavior; A Neuropsychological Theory**. Wiley, New York, 1949.
- 59 LOMO, T. The discovery of long-term potentiationo. **Philos. Trans. R. Soc. Lond. Biol. Sci.**, vol. 358, p. 617-620, 2003.
- 60 LAMEU, E. L.; MACAU, E. E.; BORGES, F. S.; IAROSZ, K. C.; Caldas, I. L.; BORGES, R. R.; PROTTACHEVICZ, P.; VIANA, R. L.; BATISTA, A. M. Alterations in brain connectivity due to plasticity and synaptic delay. **Eur. Phys. J. Spec. Top.**, vol. 227, p. 673-682, 2018.
- 61 POPOVYCH, O. V.; YANCHUK, S.; TASS, A. Self-organized noise resistance of oscillatory neural networks with spike timing-dependent plasticity. **Sci. Rep.**, vol. 3, p. 2926, 2013.
- 62 BORGES, R. R.; BORGES, F. S.; LAMEU, E. L.; BATISTA, A. M.; IAROSZ, K. C.; CALDAS, I. L.; ANTONOPOLOUS, C. G.; BAPTISTA, M. S. Spike timing-dependent plasticity induces non-trivial topology in the braino. **Neural Netw.**, vol. 88, p. 58-64, 2017.
- 63 BORGES, R. R.; BORGES, F. S.; LAMEU, E. L.; PROTTACHEVICZ, P.; IAROSZ, K. C.; CALDAS, I. L.; VIANA, R. L.; MACAU, E. E.; BAPTISTA, M. S.; GREBOGI, C.; BATISTA, A. M. Synaptic plasticity and spike synchronisation in neuronal networks. **Braz. J. Phys.**, vol. 47, p. 678-688, 2017.
- 64 BORGES, R. R.; BORGES, F. S.; LAMEU, E. L.; BATISTA, A. M.; IAROSZ, K. C.; CALDAS, I. L.; VIANA, R. L.; SANJUAN, M. A. F. Effects of the spike timing-dependent plasticity on the synchronisation in a random Hodgkin-Huxley neuronal network. **Communo. Nonlinear Sci. Numer. Simul.**, vol. 34, p. 12-22, 2016.

- 65 BUTTS, D. A.; KANOLD, O.; SHATZ, C. J. A burst-based Hebbian learning rule at retinogeniculate synapses links retinal waves to activity-dependent refinement. **PLoS Biol.**, vol. 5, p. e61, 2007.
- 66 WANG, Z.; BARUNI, S.; PARASTECH, F.; JAFARI, S.; GHOSH, D.; PERC, M.; HUSSAIN, I. Chimera in an adaptive neuronal network with burst-timing-dependent plasticity. **Neurocomputing**, vol. 406, p. 117-126, 2020.
- 67 GJORGJIEVA, J.; TOYOIZUMI, T.; EGLEN, S. J. Burst-time-dependent plasticity robustly guides on/off segregation in the lateral geniculate nucleus. **PLoS Comput. Biol.**, vol. 5, p. e1000618, 2009.
- 68 SILVEIRA, J. A. P.; PROTTACHEVICZ, R.; VIANA, R. L.; BATISTA, A. M. Effects of burst-timing-dependent plasticity on synchronous behaviour in neuronal network. **Neurocomputing**, vol. 436, p. 126, 2021.
- 69 OTA, R.; OLIVEIRA, J. C.; LCM, D.; MFD, M. Nonperiodic stimulation for the treatment of refractory epilepsy: applications, mechanisms, and novel insights. **Epilepsy Behav.**, vol. 121, p. 106609, 2021.
- 70 WANG, W. J.; ZHONG, Y. B.; ZHAO, J. J.; REN, M.; ZHANG, S. C.; XU, M. S.; XU, S. T.; ZHANG, Y. J.; SHAN, C. L. Transcranial pulse current stimulation improves the locomotor function in a rat model of stroke. **Neural Regeno. Res.**, vol. 16, p. 1229, 2021.
- 71 JABERZADEH, S.; BASTANI, A.; ZOGHI, M.; MORGAN, M.; FITZGERALD, B. Anodal transcranial pulsed current stimulation: The effects of pulse duration on corticospinal excitability. **PLoS One**, vol. 10, p. e0131779, 2015.
- 72 BOARETTO, B. R. R.; BUDZINSKI, R. C.; PRADO, T. L.; LOPES, S. R. Suppression of phase synchronization in scale-free neural networks using external pulsed current protocols. **Math. Comput. Appl.**, vol. 24, p. 46, 2019.
- 73 HANSEN, M.; PROTTACHEVICZ, R.; IAROSZ, K. C.; CALDAS, I. L.; BATISTA, A. M.; MACAU, E. E. Dynamics of uncoupled and coupled neurons under an external pulsed current. **Chaos, Solitons and Fractals**, vol. 155, p. 111734, 2022.
- 74 HAGBERG, A. A.; SCHULT, D. A.; SWART, J. **Exploring Network Structure, Dynamics, and Function using NetworkX**. Proceedings of the 7th Python in Science Conference, CA, USA, p. 11-15, 2008.
- 75 KANDAL, E. R.; SCHWARTZ, J. H.; JESSELL, T. M.; SIEGELBAUM, S. A.; HUDSPETH, A. J. **Principles of neural science**. New York: McGraw-hill, 2013.
- 76 NORTHROP, R. B. **Introduction to Dynamic Modeling of Neuro-Sensory Systems**. Biomedical Engineering, CRC Press, 2001.



- 77 BEAR, M. F.; CONNORS, B. W.; PARADISO, M. A. **Neurociências: desvendando o sistema nervoso**. Artmed Editora, 4 a Edição, 2017.
- 78 ARBIB, M. A. **The Handbook of Brain Theory and Neural Networks**. The MIT Press, Cambridge, Massachusetts, London, England, Second Edition, 2002.
- 79 BRODAL, P. **The central nervous system**. Institute of Basic Medical Sciences, Fourth Edition, 2010.
- 80 DEBANNE, D.; CAMPANAC, E.; BIALOWAS, A.; CARLIER, E.; ALCARAZ, G. Axon Physiology. **Physiological Reviews**, vol. 91, no. 2, p. 555-602, 2011.
- 81 SQUIRE, L.; BERG, D.; BLOOM, F.; DU LAC, S.; GHOSH, A.; SPITZER, N. **Fundamental Neuroscience**. Fundamental Neuroscience Series, Elsevier Science, 2008.
- 82 Free pik repository, Designed by brgfx. <https://www.freepik.com/free-vector/stem-cell-diagram-white-background-2480958.htm>.
- 83 ERMENTROUT, G. B.; Terman, D. H. Mathematical foundations of neuroscience. **Springer Science Business Media**, vol. 35, 2010. 2010.
- 84 GABRICK, E. C.; BORGES, F. S.; IAROSZ, K. C.; PROTACHEVICZ, R.; BATISTA, A. M. Dinâmica de uma rede neuronal modelada por Autômato Celular. **ENCONTRO DE PESQUISA DA FATEB e ENCONTRO DE INICIAÇÃO CIENTÍFICA, Telêmaco Borba**, vol. 2, p. 11-22, 2021.
- 85 PIKOVSKY, A.; ROSENBLUM, M.; KURTHS, J. **Synchronization: A universal concept in nonlinear sciences**. Cambridge University Press, 2001.
- 86 Synapse. <https://www.youtube.com/watch?v=uAhOdnGH5bM>.
- 87 DESTEXHE, A.; MAINEN, Z. F.; SEJNOWSKI, T. J. An efficient method for computing synaptic conductances based on a kinetic model of receptor binding. **Neural Computation**, vol. 6.1, p. 14-18, 1994.
- 88 RULKOV, F. Modelling of spiking-bursting neural behavior using two dimensional map. **Physical Review E**, vol. 65, p. 041922, 2002.
- 89 EULER, E. Solutio problematis ad geometriam situs pertinentis. **Commentarii academiae scientiarum Petropolitanae**, vol. 5, p. 128-140, 1741.
- 90 ALEXANDERSON, G. Euler and Königsberg's Bridges: A historical view. **Bulletin of the american mathematical society**, vol. 43, no. 4, p. 567-573, 2006.
- 91 WEST, D. B. Introduction to graph theory. **Prentice hall Upper Saddle River**, vol. 2, 2001.

- 92 STROGATZ, S. H. Exploring complex networks. **Nature**, vol. 410, no. 6825, p. 268-276, 2001.
- 93 OPSAHL, T.; AGNEESSENS, F.; SKVORETZ, J. Node centrality in weighted networks: Generalizing degree and shortest paths. **Soc. Netw.**, vol. 32, p. 245-251, 2010.
- 94 SARAMAKI, J.; KIVELA, M.; ONNELA, J. P.; KASKI, K.; KERTESZ, J. Generalizations of the clustering coefficient to weighted complex networks. **Physical Review E**, vol. 75, p. 027105, 2007.
- 95 COASTANTINI, G.; PERUGINI, M. Generalization of Clustering Coefficients to Signed Correlation Networks. **PloS one**, vol. 9, p. e88669, 2014.
- 96 GILBERT, N. Random Graphs. **Anno. Math. Stat.**, vol. 30, p. 1141, 1959.
- 97 WATTS, D. J. **Small worlds: the dynamics of networks between order and randomness**. Princeton University Press, 2004.
- 98 LATORA, V.; MARCHIORI, M. Efficient behavior of small-world networks. **Physical Review Letters**, vol. 87, no. 19, p. 198701, 2001.
- 99 EBEL, H.; DAVIDSEN, J.; BORNHOLDT, S. Dynamics of social networks. **Complexity**, vol. 8, no. 2, p. 24-27, 2002.
- 100 TELESFORD, Q. K.; JOYCE, K. E.; HAYASAKA, S.; BURDETTE, J. H.; LAURIENTE, J. The ubiquity of small-world networks. **Brain Connectivity**, vol. 1, no. 5, p. 367-375, 2011.
- 101 BOCCALETTI, S.; KURTHS, J.; OSIPOV, G.; VALLADARES, D. L.; ZHOU, C. S. The synchronization of chaotic systems. **Physics Reports**, vol. 366, no. 1-2, p. 1-101, 2002.
- 102 WILEY, D. A.; STROGATZ, S. H.; GIRVAN, M. The size of the sync basino. **Chaos: An Interdisciplinary Journal of Nonlinear Science**, vol.16, no. 1, p. 015103, 2006.
- 103 IVANCHENKO, M. V.; OSIPOV, G. V.; SHALFEEV, D.; KURTHS, J. Phase synchronization in ensembles of bursting oscillators. **Physical Review Letters**, vol. 93, no. 13, p. 134101, 2004.
- 104 ARENAS, A.; DIAZ-GUILERA, A.; KURTHS, J.; MORENO, J.; ZHOU, C. Synchronization in complex networks. **Physics Reports**, vol. 469, no. 3, p. 93-153, 2008.
- 105 KURAMOTO, Y. Chemical oscillations, waves, and turbulence. **Springer Science Business Media**, vol. 19, 2012.
- 106 STEVENS, S. **Psychophysics**. Transaction Publisher: New Jersey, 1975.

- 107 BORGES, F. S.; PROTACHEVICZ, R.; ANTOS, V.; SANTOS, M. S.; GABRICK, E. C.; IAROSZ, K. C.; LAMEU, E. L.; BAPTISTA, M. S.; CALDAS, I. L.; BATISTA, A. M. Influence of inhibitory synapses on the criticality of excitable neuronal networks. **Indian Academy of Sciences Conference Series**, vol. 3, 2020.
- 108 BOON, P.; VONCK, K.; DE HERD, V.; VAN DYCKE, A.; GOETHALS, M.; GOOSSENS, L.; VAN ZANDIJCKE, M.; DE SMEDT, T.; DEWAELE, I.; ACHTEN, R.; WADMAN, W.; DEWAELE, F.; CAEMAERT, VAN ROOST, J. D. Deep brain stimulation in patients with refractory temporal lobe epilepsy. **Epilepsia**, vol. 48, p. 1551, 2007.
- 109 MARIN, G.; CASTILLO-RANGEL, C.; SALOMON-LARA, L.; VEGA-QUESADA, L. A.; ZARATE-CALDERON, C. J.; BORDA-LOW, C. D.; SOTO-ABRAHAM, J. E.; CORIA-AVILA, J. A.; MANOZ, J.; GARCIA-HERNANDEZ, L. I. Deep brain stimulation in neurological diseases and other pathologies. **Neurology Perspectives**, vol. 2, p. 151-159, 2022.
- 110 Parkinsons NSW. <https://www.parkinsonsnsw.org.au/3d-software-to-improve-success-of-dbs-surgery/>.
- 111 BERLUCHHI, G.; BUCHTEL, H. A. Neuronal plasticity: historical roots and evolution of meaning. **Exp. Brain Res.**, vol. 192, p. 307, 2009.
- 112 eSchoolToday. <https://eschooldtoday.com/drug-abuse-facts/drug-use-and-the-braino.html>.
- 113 KEREPESEI, C.; SALKAI, B.; VARGA, B.; GROLMUSZ, V. The braingraph.org database of high resolution structural connectomes and the brain graph tools. **Cogno. Neurodynamics**, vol. 11, p. 483-486, 2017.
- 114 KEREPESEI, C.; SALKAI, B.; VARGA, B.; GROLMUSZ, V. How to direct the edges of the connectomes: dynamics of the consensus connectomes and the development of the connections in the human brain. **PLoS One**, vol. 11, p. e0158680, 2016.
- 115 SALKAI, B.; KEREPESEI, C.; VARGA, B.; GROLMUSZ, V. High-resolution directed human connectomes and the consensus connectome dynamics. **PLoS One**, vol. 14, p. e0215473, 2019.
- 116 FELDMAN, M. L. **Morphology of the neocortical pyramidal neuron**. Plenum Press, New York London, p. 123-200, 1984.
- 117 BANNISTER, A. Inter- and intra-laminar connections of pyramidal cells in the neocortex. **Neurosci. Res.**, vol. 53, p. 95-103, 2005.
- 118 BUZSAKI, G. **Rhythms of the brains**. Oxford: Oxford University Press, 2006.

- 119 BATISTA, C. A. S.; BATISTA, A. M.; PONTES, J. A. C.; VIANA, R. L.; LOPES, J. R. Chaotic phase synchronization in scale-free networks of bursting neurons. **Phys. Revol. E**, vol. 76, p. 016218, 2007.
- 120 PROTACHEVICZ, R.; BORGES, F. S.; LAMEU, E. L.; JI, P.; IAROSZ, K. C.; KIHARA, A. H.; CALDAS, I. L.; SZEZECH, J. D.; BAPTISTA, M. S.; MACAU, C. G. Antonopoulos, A. M. Batista, and J. Kurths, E. E. Bistable Firing Pattern in a Neural Network Model. **Front. Comput. Neurosci.**, vol. 13, p. 19, 2019.